Extreme geochemical variability through the dunitic transition zone of the Oman ophiolite: Implications for melt/fluid-rock reactions at Moho level beneath oceanic spreading centers

Mathieu Rospabé, Mathieu Benoit, Georges Ceuleneer, Florent Hodel, Mary-Alix Kaczmarek

Extreme geochemical variability through the dunitic transition zone of the Oman ophiolite: implications for melt/fluid-rock reactions at Moho level beneath oceanic spreading centers

Mathieu Rospabé [a,*], Mathieu Benoit [a], Georges Ceuleneer [a], Florent Hodel [a,b], Mary-Alix Kaczmarek [a,c]

[a] Géosciences Environnement Toulouse (GET), Observatoire Midi Pyrénées, Université de Toulouse, CNRS, IRD, 14 avenue E. Belin, F-31400 Toulouse, France

[b] Instituto de Astronomia, Geofísica e Ciências Atmosféricas, Universidade de São Paulo, 05508-900 São Paulo, Brazil

[c] Institute of Earth Sciences, University of Lausanne, Géopolis, 1015 Lausanne, Switzerland

* Corresponding author. E-mail address: mathieu.rospabe@get.omp.eu

Abstract

The Maqsad area in the Oman ophiolite exposes a >300 m thick dunitic mantle-crust transition zone (DTZ) that developed above a mantle diapir. The Maqsad DTZ is primarily made of "pure" dunites (olivine with scattered chromite and chromite seams) and "impregnated" dunites, which exhibit a significant lithological variability, including various kinds of clinopyroxene-, plagioclase-, orthopyroxene-, amphibole (hornblende/pargasite)-bearing dunites. These minerals are interstitial between olivine grains and their variable abundance and distribution suggest that they crystallized from a percolating melt. Generally studied through *in-situ* mineral characterization, the whole rock composition of dunites is poorly documented. This study reports on whole rock and minerals major and trace element

contents on 79 pure to variably impregnated dunites collected systematically along cross sections from the base to the top of the DTZ. In spite of its high degree of depletion, the olivine matrix is selectively enriched in the most incompatible trace elements such as LREE, HFSE, Th, U, Rb and Ba. These data support the view that this enrichment has been acquired early in the magmatic evolution of the DTZ, during the dunitization process itself. The dissolution of orthopyroxene from mantle harzburgites enhanced by the involvement of hydrothermal fluids produced low amounts of melts enriched in silica and in some trace elements that re-equilibrated with the olivine matrix. This pristine signature of the DTZ dunite was eventually variably altered by percolation of melts with a Mid-Ocean Ridge Basalt (MORB) affinity but displaying a wide spectrum of composition attributable to evolution by fractional crystallization and hybridization with the silica enriched, hydrated melts. The olivine matrix has been partially or fully re-equilibrated with these melts, smoothing the early strong concave-upward REE pattern in dunite. The chemical variability in the interstitial minerals bears witness of the percolation of MORB, issued from the mantle decompression melting, variably hybridized with melt batches produced within the DTZ by melt-rock reaction and poorly homogenized before reaching the lower crust. Our results lead to the conclusion that pure and impregnated dunites are end-members that recorded different stages of the same initial igneous processes: pure dunites are residues left after extraction of a percolating melt while impregnated dunites correspond to a stage frozen before complete melt extraction. Therefore dunites trace elements contents allow deciphering the multi-stage processes that led to their formation at the mantle-crust transition zone.

Keywords

Oman ophiolite; dunitic mantle-crust transition zone; trace elements; melt-rock reactions; melt percolation; refertilization

1. Introduction

The boundary between the Earth mantle and the oceanic crust is underlined by a dunitic horizon in most ophiolites worldwide, regardless the tectonic setting in which they evolved (mid-ocean ridges vs. supra-subduction zone) (e.g. Moores and Vine, 1971; Prinzhofer et al., 1980; Boudier and Coleman, 1981; Quick, 1981; Jan and Howie, 1981; Kelemen et al., 1997a; Bédard and Hébert, 1998; Ceuleneer and le Sueur, 2008; Bouilhol et al., 2009). Since dunites are observed in present-day oceans in different tectonic settings, associated to mantle harzburgites and to troctolitic-gabbroic veins and sills like in the dunitic mantle-crust transition zone (DTZ) (e.g. Arai and Matsukage, 1996; Dick and Natland, 1996; Parkinson and Pearce, 1998; Savov et al., 2005; Godard et al., 2008), it is reasonable to suppose that ophiolitic DTZ formed prior to the intra-oceanic thrusting leading to obduction.

A residual origin for dunites after very high (>40%) degrees of partial melting of the mantle (Green and Ringwood, 1967) requires unrealistic thermal regimes, at least in the modern Earth and in oceanic spreading contexts (Herzberg et al., 1983). Alternatively, dunite may result from the accumulation of olivine grains issued from fractional crystallization from a melt sufficiently rich in Mg to remain during a significant time in the fractionation field of olivine alone (+/- spinel) (Bowen, 1915; O'Hara, 1965; Elthon, 1979). Finally, dunite may be replacive after interaction ("reactional melting") between melts and peridotite in dry (Bowen, 1927; Berger and Vannier, 1984) or hydrated systems (Bowen and Tuttle, 1949). The interaction between harzburgite and a melt undersatured in silica accounts for the formation of dunite through the dissolution of pyroxenes, leading to the enrichment in silica of the melt with concomitant crystallization of olivine (Dick, 1977; Quick, 1981; Kelemen, 1990; Kelemen et al., 1992). Petrological evolutions across a densely sampled cross section along a

330 m thick DTZ of the Oman ophiolite revealed that the DTZ does essentially but not exclusively derive from melt-peridotite interaction, its shallowest part (topmost 50 m) showing fractional crystallization trends (Abily and Ceuleneer, 2013).

In the melt-rock reaction model, it was proposed that reactional melting and orthopyroxene consumption leads to high intergranular permeability enhancing the efficiency of melt extraction from the mantle (Ortoleva et al., 1987; Daines and Kohlstedt, 1994; Kelemen et al., 1995a; Kelemen et al., 1997b). In this way, the DTZ appears to be a reactive interface where melts are focused, transformed and potentially accumulated, then distributed beneath the mid-ocean ridge. Crystallization associated to melt migration through the mantle-crust transition zone accounts for the wide diversity of lithological facies observed in the DTZ. Dunites evolve from “pure dunites”, i.e. compacted at very high temperature when complete melt extraction occurred, to “impregnated dunites”, highly refertilized before incipient cooling and that potentially leads in extreme cases to the formation of hybrid olivine-rich troctolites or plagioclase-bearing wehrlites (e.g. Arai and Matsukage, 1996; Abily and Ceuleneer, 2013; Sanfilippo and Tribuzio, 2013a). Although interstitial minerals in ophiolites or abyssal DTZ are regularly found in equilibrium with melts that fed the overlying crust (e.g. Drouin et al., 2009; Ghosh et al., 2014; Nicolle et al., 2016), the Oman ophiolite DTZ was also percolated by melts with more exotic compositions (Koga et al., 2001) that, for a part of them, may be attributable to hybridization with a hydrothermal fluid component (Rospabé et al., 2017). Especially the presence of orthopyroxene, amphibole, garnet and diopsides both interstitially between olivine grains and in inclusion in chromite calls for early, high temperature, hydration of the DTZ. In this frame, to define the origin of the DTZ has direct implications on melt generation, transfer and evolution from the mantle to the crust, as well as on the deep hydrothermal circulations that may influence both the chemical exchanges and the thermal

100 structure of the oceanic lithosphere.

101

102 Most geochemists use the trace element contents of interstitial clinopyroxene and plagioclase
103 (if any) scattered in dunites to build petrological scenario (e.g. Kelemen et al., 1995a; Nicolle
104 et al., 2016; Akizawa et al., 2016a). However, it concerns actually the genesis of
105 crystallization products from melt fractions that travelled through the dunites, which might be
106 risky to extrapolate to the genesis of the dunitic matrix itself. Very few whole rock analysis or
107 olivine trace element contents are available due to their very low content in olivine. The
108 sporadic studies providing trace elements data on dunite show that re-equilibration processes
109 occurred between the olivine matrix, selectively enriched in some trace elements, and the
110 melts percolating interstitially between olivine grains (e.g. Godard et al., 2000; Gerbert-
111 Gaillard, 2002; Sanfilippo et al., 2014, 2017).

112

113 To better constrain the processes leading to the formation of both pure and impregnated
114 dunitic products constituting the DTZ as well as to their chemical signature, we combined
115 major and trace elements in whole rock and in mineral phases for 79 samples of dunite from
116 the Oman ophiolite mantle-crust transition zone. We show that the important chemical
117 variability recorded by the dunites at Moho level is issued from a combination of harzburgite
118 dunitization, re-equilibration associated to melt percolation, and refertilization from unmixed
119 and contrasted MORB-derived melt batches variably hybridized with hydrous fluids.

120

121 **2. Geological background**

122 *2.1. Geology of the Oman ophiolite*

123 The Oman ophiolite exposes a 30.000 km^2 remnant of the Tethyan Ocean. Its creation
124 occurred ~95-97 million years ago (Tilton et al., 1981; Tippit et al., 1981; Rioux et al., 2012)

and was directly followed by an oceanic detachment close to the ridge axis that eventually led to its obduction on the Arabian margin (Lanphere, 1981; Boudier et al., 1985; Boudier et al., 1988; Montigny et al., 1988). The synoptic mapping of mafic-ultramafic dykes cropping out in the mantle section (Python and Ceuleneer, 2003; Python et al., 2008) revealed that two main magmatic suites contributed to the igneous evolution of the ophiolite: (1) a MORB suite mostly present in the southeastern massifs of the ophiolite (Nakhl, Sumail and Wadi Tayin) and in some restricted areas in the north, and (2) a more widespread depleted-andesitic type attributed either to subduction or to hydrated re-melting of the shallow lithosphere during spreading (Pearce et al., 1981; Benoit et al., 1999; Python and Ceuleneer, 2003; Yamasaki et al., 2006; MacLeod et al., 2013) (Fig. 1a).

Along the Oman ophiolite, spatially constrained vertical flow structures within the mantle section were interpreted as former asthenospheric diapirs distributed along the oceanic ridge (Ceuleneer et al., 1988; Nicolas et al., 1988; Jousselin et al., 1998; Nicolas et al., 2000). The Sumail massif, focus of the present study, exposes in the Maqsad area a well preserved paleo mantle diapir and its associated N130 paleo-spreading center (Ceuleneer, 1986; Ceuleneer et al., 1988; Ceuleneer, 1991; Jousselin et al., 1998). This structure is located in the central part of the largest (80 × 25 km) MORB district of Oman (Python and Ceuleneer, 2003) (Fig. 1). The MORB affinity has been evidenced by the crystallization sequence and confirmed by trace elements and isotopic data on both mantle and crustal rocks (Benoit et al., 1996; Ceuleneer et al., 1996; Godard et al., 2000; Koga et al., 2001; Godard et al., 2003; Clénet et al., 2010).

2.2. The dunitic transition zone around the Maqsad diapir

The thickness of the DTZ reaches 300 to 350 m above the central part of the Maqsad mantle

diapir (Rabinowicz et al., 1987; Boudier and Nicolas, 1995; Jousselin and Nicolas, 2000; Abily and Ceuleneer, 2013) and thins progressively off-axis due to tectonic transposition by mantle plastic flow as it diverges from the diapir (Ceuleneer, 1991). In this area the DTZ was mainly described as the uppermost part of the mantle, modified after complete orthopyroxene consumption resulting from MORB-peridotite interaction (Godard et al., 2000; Gerbert-Gaillard, 2002), while its upper part (top most ~50 m) displays all the characteristic of cumulates (Abily and Ceuleneer, 2013). The interstitial plagioclase and clinopyroxene located between olivine grains exhibit chemical signature in good agreement with a fractionation from a percolating MORB (Koga et al., 2001; Abily and Ceuleneer, 2013; Nicolle et al., 2016). It was also recently evidenced that some horizons of the DTZ contain interstitial orthopyroxene and pargasite that support the percolation of a hybrid liquid, i.e. a blend of variably evolved MORB and of hydrous silica-rich liquids (Rospabé et al., 2017). The ubiquitous occurrence of hydrothermal diopside and grossular, both in interstitial position between olivine grains and enclosed in disseminated chromite together with orthopyroxene, pargasite, biotite and aspidolite, suggests them as primary high temperature features and further challenges the pure igneous origin of the DTZ. According to our observations, they are not systematically associated to cracks affecting chromite grain, as would be expected if they were low temperature alteration products resulting from serpentinization and Ca-rich metasomatism having affected mafic and ultramafic rocks (e.g. Palandri and Reed, 2004; Python et al., 2011; Akizawa et al., 2016b) (see also Tamura et al., 2014). The possible involvement of high temperature hydrothermal fluids during the magmatic stage that edified the DTZ allows reconsidering the former hypothesis of a hydrothermal origin for dunites, originally proposed by Bowen and Tuttle (1949).

3. Methods

175 *3.1. Sampling strategy*

176 The Sumail massif was slightly tilted during the Miocene uplift of the Djebel Akhdar. Its
177 regional dip does not exceed 10° to the SE. For this reason, to perform sampling along
178 distributed cross sections is a straightforward way to reconstruct the three-dimensional
179 structuration of the DTZ around the Maqsad diapir and its associated paleo-ridge axis. In this
180 study we report on whole rock and mineral major elements and whole rock trace elements for
181 79 samples, and on interstitial clinopyroxenes trace elements for 11 impregnated dunites.
182 Samples were collected systematically every 10 to 20 m vertically along four cross sections
183 (Fig. 1b). Their location and mineral contents are presented in Table 1.

184

185 *3.2. Analytical methods*

186 *In situ* mineral major element concentrations were acquired by electron microprobe using a
187 Cameca SX 100 (Microsonde Ouest, Brest, France) and a Cameca SXFive (Centre de
188 MicroCaractérisation Raimond Castaing, Toulouse, France) with a 20 kV accelerating
189 voltage, a beam current of 20 nA, an electron beam diameter of 1 μm for all analyses and a
190 counting time of 10 s on peak for each element and 5 s on backgrounds on both sides of the
191 peak. *In situ* clinopyroxene trace element concentrations were obtained by laser ablation-
192 inductively coupled plasma-mass spectrometry (LA-ICP-MS) at the Institute of Earth
193 Sciences, University of Lausanne (Switzerland). We used a NewWave UP-193 ArF
194 Excimer based laser ablation system coupled with a Thermo Scientific™ ELEMENT XR™
195 high resolution ICP-MS. Spot size ranged between 75 and 100 μm and operating conditions
196 were a 20 Hz pulse rate and an energy density of 6.0 J/cm^2. The SRM612 NIST was used as
197 external standard following the values proposed by Jochum et al. (2011) and ^{29}Si was used as
198 internal standard.

199

Whole rock major element concentrations were obtained by X-ray Fluorescence Spectrometry at the Central Analytical Facilities, Stellenbosch University (South Africa). Whole rock trace element concentrations were acquired on a Thermo Scientific™ ELEMENT XR™ HR-ICP-MS at the Géosciences Environnement Toulouse laboratory (Observatoire Midi-Pyrénées), Université of Toulouse III. The sample preparation consisted in a HF-$HClO_4$ digestion procedure (Yokoyama et al., 1999) combined with a thulium addition (Barrat et al., 1996). The concentrations in Li and Large Ion Lithophile Elements (LILE; Rb, Sr, Cs and Ba) and of most of transition elements (Cr, Mn, Co, Ni, Cu, Zn) and Ga were acquired after a direct digestion/dilution method. Sc, V, Rare Earth Elements (REE) and Y, High Field Strength Elements (HFSE; Zr, Hf, Nb, Ta, Ti) and U, Th and Pb contents were determined after the double coprecipitation procedure detailed in Rospabé et al. (2018). BHVO-2 was used as calibrator following the values proposed by Barrat et al. (2012). The yield was monitored and concentrations calculated using the Tm anomaly appearing in the samples REE pattern (Barrat et al., 1996). The international rock standards UB-N (serpentinite) and DTS-2B (dunite) were analysed as unknown during the course of this study. They are given in Appendix A together with the samples major and trace element compositions.

4. Lithological diversity in the Maqsad DTZ

Olivines exhibit a recrystallized equigranular mosaic texture with frequent triple junctions at 120° (Fig. 2a). Its average grain size is about 1 mm. All samples are affected to some degree by serpentinization, which ranges from about 30 to 60%. Submillimeter round-shaped chromite grains are interstitial between olivine grains. They are generally disseminated but chromite schlierens occur in some samples. Small grains of clinopyroxene are also frequently observed at olivine triple junctions or along the olivine grain rims, with a grain size no larger than few tens of microns. Samples with less than 0.5% of clinopyroxene are considered as

225 “pure dunites” (38 samples).

226

227 The remaining 41 samples contain well-developed oikocrystic of clinopyroxene and/or other
228 interstitial minerals. These interstitial phases are classically interpreted as crystallization
229 products fractionated from a melt that percolated through the dunitic matrix and are referred
230 to as “impregnated dunites” (Benn et al., 1988; Boudier and Nicolas, 1995; Koga et al., 2001;
231 Abily and Ceuleneer, 2013). Two contrasted clinopyroxene compositions are observed; one
232 consistent with an igneous origin and the other one calling for crystallization from
233 hydrothermal fluids or water-rich melts (Python et al., 2007; Rospabé et al., 2017).
234 Accordingly, we use "clinopyroxene" and "diopside" to distinguish clinopyroxene with
235 igneous and hydrothermal origin respectively. Clinopyroxene is the most common
236 impregnating phase (14 samples are cpx-bearing dunites). Its texture changes with its modal
237 abundance, from small interstitial at olivine grains boundaries (up to hundreds microns width
238 in size) to oikocrystic crystals (millimeter to up to centimetre in size) (Fig. 2b). Smaller
239 interstitial diopsides are also sometimes observed both in pure and impregnated dunites,
240 showing different texture and chemical content than the clinopyroxene oikocrysts (Fig. 2c).
241 Plagioclase appears as a well-developed interstitial intercumulus phase, generally as
242 oikocrysts (Fig. 2d), and is regularly associated to clinopyroxene, characterizing the pl/cpx-
243 bearing dunites (14 samples). Plagioclase-bearing cpx-free dunites are rarely observed (one
244 sample only). Plagioclase/olivine contacts are also regularly underlined by a clinopyroxene
245 corona. In addition to clinopyroxene and plagioclase, the dunites collected in the DTZ from
246 the Maqsad area show orthopyroxene oikocrysts in pl/cpx-bearing dunites (7 samples) (Fig.
247 2e), and amphibole, observed as subhedral crystals in few samples with no preference to the
248 other minerals present (7 samples) (Fig. 2f). Interstitial subhedral grossular garnet was
249 observed in 12 impregnated dunites (Rospabé et al., 2017). All these interstitial minerals are

also present as round-shaped primary inclusions in chromite grains together with micas (phlogopite and aspidolite), the latter being never observed interstitially within the dunitic matrix.

5. Results

5.1. Whole rock major and minor elements

The dunites from the DTZ plot above the mantle fractionation array in the MgO/SiO_2 vs. Al_2O_3/SiO_2 diagram (Fig. 3a). Pure dunites and slightly impregnated ones (<5% of cpx or cpx + pl) exhibit a more refractory characteristic than the most depleted harzburgites from the mantle section with higher MgO/SiO_2 (>1.1) and lower Al_2O_3/SiO_2 (<0.02) ratios. Impregnated samples are generally characterized by a progressive decrease of MgO/SiO_2 and an increase of Al_2O_3/SiO_2 that reflects an increasing amount of clinopyroxene and plagioclase. The loss on ignition (LOI) is comprised between 6.9 and 10.9 wt.% for pure dunites and 4.7 and 10.8 wt.% for impregnated dunites, and reflects primarily the degree of serpentinization that is similar in both dunite types (Appendix A). The variation of FeO and MgO in pure and slightly impregnated dunites perfectly mimics the stoichiometric variation of the olivine Fe-Mg composition (FeO + MgO = 66.67 in mol%) while other higher impregnated samples contain a lower MgO content similar to mantle harzburgites (mainly ~43-47 wt.%) (Fig. 3b).

Low CaO and Al_2O_3 also characterize the pure and slightly impregnated dunites with concentrations lower than 1 wt.% (Fig. 3c). The higher CaO and Al_2O_3 contents are strongly correlated to the abundance of impregnating minerals. The modal proportion of clinopyroxene controls the CaO content that increases fast with increasing amount of cpx ($Al_2O_3/CaO<1$ in cpx-bearing dunites) while plagioclase and amphibole exert the main control on the Al_2O_3

content in other impregnated dunites ($Al_2O_3/CaO>1$).

In pure dunites the Mg# (100 × molar Mg/(Mg + Fe_{total})) is more variable (from 86 to 92.3, except a pure dunite containing schlierens of chromites with a whole rock Mg# = 83.4) than in impregnated dunites (from 87.2 to 90.9) and peridotites from the mantle section (from 89.8 to 91.6). The dunites from the DTZ also display a much more variable Ni (1207-2870 μg/g) and a higher Co (110-155 μg/g) contents than mantle peridotites (Ni = 1747-2671 μg/g; Co = 95-122 μg/g) (Fig. 3d and 3e). These compositions are not clearly related to the degree of impregnation minerals with high Ni and Co concentrations also observed in the most impregnated samples.

5.2 Mineral major elements

The Fo in olivine (100 × molar Mg/(Mg + Fe_{total})) in dunites from the DTZ generally decreases from 92.5 to 87.8 concomitantly with the NiO content (0.45 to 0.19 wt.%) (Fig. 4a). This compositional range is broader than in the peridotites from the mantle section (89.5<Fo<92.1; 0.25<NiO<0.53 wt.%). The CaO content in olivine, mainly <0.05 wt.% in mantle harzburgites, reaches 0.32 wt.% in the DTZ. Higher CaO values are generally observed in olivine grains from pure dunites, also displaying the lower Fo and NiO contents (Fig. 4b), and may consequently not be attributed to re-equilibration with other CaO-rich minerals. Fo in olivine and Mg# in whole rocks are highly correlated (Fig. 4c).

The Cr# (100 × molar Cr/(Cr + Al)) variation range in chromite is more restricted in dunites from the DTZ (43.3-63.4) than in harzburgites from the mantle section (20.6-70). Cr# gently decreases with the Fo and progressively shifts from the olivine-spinel mantle array (OSMA) (Arai, 1987, 1994) (Fig. 4d). Mg# (100 × molar Mg/(Mg + Fe^{2+})) in chromite is quite similar

between the different types of dunite (43.3-63.4) while the TiO_2 content is on the contrary much more variable depending on the host lithological facies (Fig. 4e), being lower (0.20-0.60 wt.%) in pure dunites than in impregnated ones (mainly comprised between 0.15 and 0.9 wt.% and occasionally reaching 1.3 wt.%). On the contrary YFe^{3+} (100 × molar Fe^{3+}/(Cr + Al + Fe^{3+})) is slightly higher in chromite from the pure dunites (Appendix B).

Minute clinopyroxenes were observed at the triple junction of olivine grains in what we defined as pure dunites. They exhibit a variable Mg# (86.9-94.2) and a CaO content exceeding 24.5 wt.% that contrast with the clinopyroxene oikocrysts from the impregnated dunites (Mg# = 89.6-92.9; CaO = 21.1-24.8 wt.%) (Appendix B). All the clinopyroxenes display a wide variation range in TiO_2 (0.16-0.71 wt.%) (Fig. 4f), Cr_2O_3 (0.79-1.32 wt.%) and Al_2O_3 (2.6-4.9 wt.%) (Appendix B). Zoning was observed in few clinopyroxenes only, with the concomitant increase of Mg#, SiO_2 and TiO_2 together with the decrease of Al_2O_3 and Cr_2O_3 from the core to the rim. Small interstitial diopside composition ranges between igneous and hydrothermal end-members, with higher Mg# and lower TiO_2 (Fig. 4f), Cr_2O_3 and Al_2O_3 contents (see also Rospabé et al., 2017).

Oikocrystic orthopyroxene grains observed in interstitial position in dunites present a high TiO_2 content (0.15-0.23 wt.%), specific to the dunites from the Maqsad area (Rospabé et al., 2017) (Appendix B). They display Mg# and Al_2O_3 contents varying from 88.8 to 90.8 and 1.15 to 2.22 wt.% respectively. As clinopyroxene, orthopyroxene rarely exhibits zoned compositions with the increase of SiO_2 concomitantly to the decrease of Al_2O_3, and Cr_2O_3 from the core to the rim. Mg# is quite variable as MgO and FeO both increase with SiO_2.

Plagioclase was not systematically analysed in each pl-bearing dunites due to its higher

degree of alteration than other phases. It presents rather primitive compositions in (opx/)pl/cpx-bearing dunites (An (100 × molar Ca/(Ca + Na + K)) = 86.3-90.1) while being more evolved in one amphibole/pl/cpx-bearing dunite (An = 74.6) (Appendix B).

Interstitial amphiboles in the studied samples are pargasites, pargasitic- or edenitic-hornblende. They display Mg# ranging from 85.7 to 91.4 and extremely variable Al_2O_3 (11.0-16.3 wt.%), Na_2O (1.98-3.75 wt.%), TiO_2 (0.02-1.24 wt.%) and Cr_2O_3 (0.01 to 1.81 wt.%) contents (Appendix B).

5.3. Whole rock trace elements

The dunites from the DTZ exhibit variable trace element compositions (Appendix A). Pure dunites are highly depleted in lithophile trace elements with concentrations below both the chondritic and the Primitive Mantle (PM) values (mostly comprised between 0.001 and 0.1 times the PM concentrations). Pure dunites are characterized by U- or V-shape REE chondrite-normalized patterns (Fig. 5a), reflecting the major MREE (Sm, Eu and Gd) depletion relative to LREE (La_{CN}/Sm_{CN} <3.76; 1.9 in average) and HREE (0.04< Gd_{CN}/Yb_{CN} <0.28). We define the U- or V-shape appellation depending on the presence or absence of negative Eu anomaly. The $(Eu/Eu^*)_{CN}$ ratio ranges between 0.22 and 1 in 29 samples, while 9 samples exhibit a positive Eu anomaly with $(Eu/Eu^*)_{CN}$ <2.4 ($(Eu/Eu^*)_N = Eu_{CN}/\sqrt{(Sm_{CN} \times Gd_{CN})}$). Pure dunites display relative homogeneous HREE concentrations (Yb_{CN} = 0.10-0.24) in comparison to more variable MREE (0.005< Gd_{CN} <0.059; 0.004< Sm_{CN} <0.065) and especially LREE (0.004< La_{CN} <0.17). The depletion from HREE to MREE is not linear with several samples exhibiting instead concave-upward patterns with a progressive Gd_{CN}/Dy_{CN} increase for a constant Er_{CN}/Yb_{CN}. Pure dunites U-shaped PM-normalized multi-elements patterns exhibit significant enrichments in LILE, Th, U, Nb and Ta relative to LREE

(Rb_{PMN}/La_{PMN} = 1.5-85; Th_{PMN}/La_{PMN} = 0.7-5.3) and strong Pb and Sr positive anomalies similar to mantle peridotites (2.19< Pb_{PMN}/Ce_{PMN} <1294) (Fig. 5b). Zr and Hf are generally enriched relative to MREE (Zr_{PMN}/Sm_{PMN} = 0.6-27; 2.9 in average) as well as Ti that displays a strong positive anomaly (1.3< Ti_{PMN}/Gd_{PMN} <76).

Cpx-bearing dunites exhibit variable REE and multi-element patterns partly attributable to variations in the interstitial clinopyroxene content. Slightly impregnated ones (<5% cpx) exhibit linear LREE-depleted or slightly concave-upward REE patterns (La_{CN}/Yb_{CN} = 0.06-0.97) with similar HREE concentrations (Yb_{CN} = 0.12-0.29) and more restricted LREE and MREE variation ranges (La_{CN} = 0.01-0.23; Gd_{CN} = 0.02-0.12) than pure dunites (Fig. 5c). Dunites containing a higher amount of clinopyroxene have higher HREE contents (Yb_{CN} = 0.56-0.83). They exhibit clear convex-upward patterns with a nearly flat slope of the HREE segment (Gd_{CN}/Yb_{CN} = 0.74-0.85) followed by a progressive depletion from MREE to LREE (La_{CN}/Sm_{CN} = 0.06-0.09). It is worth noting that the cpx-bearing dunites display La and Ce contents within the variation range of pure dunite (La_{CN} = 0.01-0.23). This observation may be extended to other incompatible trace elements like Th, U, HFSE that are not more concentrated in cpx-bearing dunites than in pure dunites, excepting one sample that displays spectacular HFSE positive anomalies (Fig. 5d). Cpx-bearing dunites exhibit similar enrichment in LILE relative to LREE and the same strong positive Pb and Sr anomalies than in pure dunites. The positive Ti anomaly observed for the slightly impregnated samples disappears for the more impregnated ones in which the Ti content is buffered around 0.25 times the PM value.

The pl-bearing dunite displays a W-shaped REE pattern with strong depletion in MREE (Sm_{CN} = 0.005; Gd_{CN} = 0.003) relative to LREE (La_{CN}/Sm_{CN} = 4.3) and HREE (Gd_{CN}/Yb_{CN} =

0.002) bordering a strong positive Eu anomaly ($(Eu/Eu^*)_{CN}$ = 54) (Fig. 5e). Other pl/cpx-bearing chondrite-normalized REE patterns evolve from concave-upward to convex upward with the increasing amount of clinopyroxene. This evolution is accounted by a progressive decrease of the HREE segment slope (Gd_{CN}/Yb_{CN} from 0.17 to 0.63). They are also characterized, in regard to pure and cpx-bearing dunites, by higher Li and Rb contents, a higher range of Cs, a well depletion in their Th and U contents, and a slighter positive Pb anomaly (Fig. 5f).

Opx/pl/cpx-bearing dunites and amphibole-bearing dunites (± opx, pl and cpx) have REE contents similar to pl/cpx-bearing dunites with patterns intermediate between highly impregnated pl-bearing and cpx-bearing dunites (Fig. 5g). They also display similar PM-normalized multi-elements patterns than pl/cpx-bearing dunites, with Th, U, and with few exceptions Nb and Ta contents similar to LREE (averaged Th_{PMN}/La_{PMN} = 0.9) (Fig. 5h).

5.4. Clinopyroxene minor and trace elements

Trace elements concentrations were obtained for unzoned crystals of clinopyroxene in 11 impregnated dunites (2 cpx-bearing, 6 pl/cpx-bearing, 3 opx/pl/cpx-bearing, and 1 amph/opx/pl/cpx-bearing). Their composition is homogeneous within a given sample. In clinopyroxenes, lower trace elements contents are observed in the amph/opx/pl/cpx-bearing dunite while higher contents much characterize cpx-bearing dunites; clinopyroxenes in (opx/)pl/cpx-bearing dunites display both low and high trace elements concentrations. Regarding the chondrite-normalized REE patterns, all the clinopyroxenes are depleted in LREE relative to MREE (La_{CN}/Sm_{CN} = 0.03-0.32) and the slope in HREE is highly variable, from strongly positive to moderately negative (Gd_{CN}/Yb_{CN} = 0.61-2.28) (Fig. 6a). The most LREE-depleted patterns are rather observed in (amph/)opx/pl/cpx-bearing dunites whatever

400 the REE concentrations, while the less depleted ones are observed in cpx-bearing dunites.
401 Negative anomalies in Nb and Ta (Nb_{PMN}/La_{PMN} = 0.08-1) relative to LREE and in Zr and Hf
402 relative to MREE (Zr_{PMN}/Sm_{PMN} = 0.14-0.43) are systematically observed whatever the host
403 lithology (Fig. 6b). With few exceptions, negative anomalies in Pb and Sr relative to LREE-
404 MREE are also observed as well as in Ti for the most enriched clinopyroxenes.
405
406 **6. Discussion**
407 The dunitic transition zone from the Maqsad area exposes various types of dunites,
408 characterized from their mineralogical content (Boudier and Nicolas, 1995; Koga et al., 2001;
409 Abily and Ceuleneer, 2013; Rospabé et al., 2017) and from their geochemical diversity within
410 each lithological facies. Previous studies proposed different processes to explain the
411 formation of pure and impregnated dunites and/or their geochemical signature: (1)
412 serpentinization or weathering, (2) fractional crystallization and accumulation of olivine and
413 other minerals, (3) melt-rock reactions comprising harzburgite reactional melting and re-
414 equilibration related to melt percolation and, (4) refertilization associated to melt transport. In
415 the next sections we will discuss the relative influence of each process in regard to the
416 geochemical variations revealed by our study, then we will propose a more general model for
417 the Maqsad DTZ genesis.
418
419 *6.1. Serpentinization or secondary weathering effects*
420 The dunites are partly serpentinized with a serpentine abundance of about 40 to 50% in
421 average, according to thin sections observation and loss of ignition (LOI) values.
422 Serpentinization is known to be nearly isochemical regarding the bulk rock major element
423 concentrations (e.g. Coleman and Keith, 1971; Deschamps et al., 2013). In our samples, the
424 LOI is not or poorly correlated with any major element contents attesting that the

425 serpentinization did not extensively affect bulk rock major element concentrations (see also
426 Rospabé, 2018). More specifically, the samples plot above the terrestrial array in the
427 MgO/SiO_2 vs. Al_2O_3/SiO_2 diagram (Fig. 3a) and do not show any evidence for MgO loss or
428 SiO_2 enrichment as reported in pervasively serpentinized abyssal peridotites or talc-bearing
429 serpentinites (Snow and Dick, 1995; Bach et al., 2004; Paulick et al., 2006; Boschi et al.,
430 2008; Malvoisin, 2015). The perfect consistency between the Fo in olivine and the Mg# in
431 whole rock (Fig. 4c) further demonstrates the absence of influence of serpentinization on the
432 bulk dunite major element compositions.
433
434 Regarding trace elements, with few exceptions, the La content is strongly correlated to the Th
435 content, in both pure and impregnated dunites (Fig. 7a). The Th, as well as HFSE, are
436 immobile during post-magmatic aqueous alteration (You et al., 1996; Kogiso et al., 1997;
437 Niu, 2004; Paulick et al., 2006). Thus, correlated enrichments of La with Th testify that LREE
438 enrichments derived from magmatic processes, as seen in mantle harzburgites from the
439 Sumail massif (Godard et al., 2000; Gerbert-Gaillard, 2002). A poorer but significant
440 correlation exists between HFSE (Zr, Hf, Nb, Ta) and U contents on one hand and Th and
441 LREE contents on the other (Fig. 7b, c and d). Rb and Ba seem to be vaguely correlated to
442 HFSE in pure dunites (especially to Zr and Hf) as well as to Th (Fig. 7e and f) and thus were
443 probably enriched during an initial igneous stage before being potentially affected again
444 during secondary weathering processes. Other LILE, such as Sr, and Pb contents are not
445 correlated to the LOI but the absence of correlation with Th suggests that their enrichment
446 could be related to a secondary alteration/serpentinization processes post-dating the igneous
447 history. This is confirmed by the fact that all the dunitic bulk rock analyses from the DTZ
448 exhibit strong positive Sr and Pb anomalies, while interstitial igneous clinopyroxenes exhibit
449 the opposite negative Sr and Pb anomalies. These trace element evolutions in regard to

immobile elements have been already described in Oman ophiolite mantle harzburgites (Gerbert-Gaillard, 2002). The co-variations of Th, U, LREE and HFSE at least may thus be interpreted in the framework of igneous processes.

6.2. Cumulative origin

A cumulative origin for dunites (Bowen, 1915; Bowen and Tuttle, 1949; O'Hara, 1965; Elthon, 1979) implies to preserve a high-Mg parental melt in the crystallization field of the single olivine (+/- spinel) during differentiation. This is quite problematic to account for thick layers (several hundred meters or large bodies of dunites), and the production of such high temperature melts is inconsistent with the inferred thermal conditions in the present day Earth interior (Verhoogen, 1954; McKenzie and Bickle, 1988; Tilley et al., 2007). However, it was proposed that the shallowest part of the Maqsad DTZ, where both Fo and NiO in olivine decrease together upsection, was generated by olivine crystallization and accumulation while the main part of the DTZ was a residue of reaction melting (Abily and Ceuleneer, 2013).

Dunites from the Maqsad DTZ exhibit Ni and Co contents that are much closer to the mantle peridotites compositions (Fig. 3d and 3e) than to the most primitive troctolite cumulates cropping out within the mantle harzburgitic section in the Maqsad area (Ni < 650 µg/g; Co < 40 µg/g; Benoit et al., 1996). This observation, together with the absence of clear correlation between Mg# and Ni in whole rock (Fig. 3d), the negative correlation between Mg# and Co in whole rock (Fig. 3e), and with the consistent compositional variations between the different types of dunites, suggests that both pure and impregnated dunites cannot be related by fractional crystallization from a common parent melt. Regarding the pure dunites, a pure cumulative origin does not account for the normalised U-/V-shaped REE patterns (Fig. 5a and 5b). The enrichment in LREE relative to MREE is not predicted by REE partition coefficients

between olivine and melt (Frey et al., 1978; McKenzie and O'Nions, 1991; Kelemen et al., 1993; Hauri and Hart, 1995; Lee et al., 2007; Sun and Liang, 2014) and may better be explain by melt-rock reactions leading to peridotite metasomatism (e.g. Navon and Stolper, 1987; Godard et al., 1995; Vernières et al., 1997). Models presented in Appendix C evidence that the olivine matrix hosting impregnations exhibit similar REE patterns than for whole rock pure dunites, with the same range of variability. In this way, impregnated dunites may be definitely interpreted as hybrid lithologies, made of a mantle-derived olivine matrix associated to other minerals crystallized during melt percolation (e.g. Rabinowicz et al., 1987; Benn et al., 1988; Boudier and Nicolas, 1995; Koga et al., 2001; Abily and Ceuleneer, 2013; Rospabé et al., 2017). The modelling allows us to conclude that the whole rock trace element signatures of impregnated dunites result from a blend of three main variables: the amount of impregnating mineral phases and their chemical signatures as expected, but also the composition of the dunitic matrix itself (Appendix C).

6.3. Melt-rock reaction product: dunitization and melt transport

6.3.1. State of melt-rock reactions leading to incompatible trace element enrichments in mantle peridotites

Incompatible trace element enrichments in peridotites, as U-shaped REE patterns, are documented in numerous peridotites from various tectonic settings, from ophiolitic and orogenic massifs (e.g. Prinzhofer and Allègre, 1985; Bodinier et al., 1990; Gruau et al., 1998; Bouilhol et al., 2009) to abyssal peridotites at mid-ocean ridges (Niu, 2004; Godard et al., 2008) or in forearc context (Parkinson and Pearce, 1998). It has been proposed that melt-rock reactions may lead to some chromatographic effects such as melt-peridotite re-equilibration or to trapped melt between olivine and pyroxene grains. This can be accounted for by (1) a two-stages process involving mantle partial melting later percolated by a LREE-enriched melt (i.e.

cryptic metasomatism in the peridotitic matrix without mineralogical reaction) (Navon and Stolper, 1987) or, (2) a single-stage process by combining partial melting (or melt-rock reaction at increasing melt mass; Vernières et al., 1997) and melt transport concomitantly, leading to a MREE depletion relative to HREE whereas LREE remain constant (Godard et al., 1995). In the Oman ophiolite, U-shaped REE patterns were described in mantle harzburgites (Godard et al., 2000; Gerbert-Gaillard, 2002; Girardeau et al., 2002; Le Mée et al., 2004; Monnier et al., 2006; Hanghøj et al., 2010), especially in the Maqsad diapir area where it is attributed to an association between partial melting, deformation related to mantle flow and MORB percolation (Godard et al., 2000; Gerbert-Gaillard, 2002).

6.3.2. Extreme trace elements enrichments in DTZ dunites: an early dunitization-related signature

The melt-rock reaction leading to dunite formation from a harzburgite through orthopyroxene dissolution is expected to result in a high intergranular permeability of the dunite, that becomes a porous media for efficient melt transfer and extraction (Toramaru and Fujii, 1986; Kelemen et al., 1995b). Dunite channels and horizons, filled or not with troctolitic cumulates, have been mapped within the Maqsad mantle section and interpreted in terms of frozen compaction waves (Ceuleneer et al, 1996; Rabinowicz and Ceuleneer, 2005). They are common features in the Maqsad diapir but not significant in terms of volume. Hence, it is unlikely that the DTZ formed by the transposition in the solid state of such dunitic bodies generated at greater depth, especially since the DTZ dunites do not show any sign of deformation. They better represent the final *in situ* reacting residue of complete dunitization of the uppermost few hundred meters of the mantle induced by melt migration and extraction. Regarding REE, pure dunites from the DTZ display lower HREE, similar and more variable MREE, and higher and more variable LREE contents than harzburgites from the Maqsad

525 mantle section (Fig. 5a) (Godard et al. 2000; Gerbert-Gaillard, 2002). The lower HREE
526 content is in good agreement with a more refractory signature, i.e. depleted, following the
527 complete resorption of orthopyroxene. However, their LREE, Zr, Hf and Th contents are
528 systematically higher than in mantle harzburgites, as Nb, Ta and U in many cases (Fig. 5a and
529 5b). Considering a reacting melt with MORB-like affinities (e.g. Ceuleneer et al., 1996;
530 Benoit et al., 1996; Kelemen et al., 1997a; Abily and Ceuleneer, 2013), these signatures are
531 inconsistent with a genesis at the expense of the surrounding harzburgites alone following the
532 single-stage process described above (Godard et al., 1995; Vernières et al., 1997). Moreover,
533 the occurrence of interstitial minerals implies that the percolating melt suffered crystallization
534 after the harzburgite dunitization, associated to the last stage of percolation during the cooling
535 of the system. Then, one can envision the overprinting of two- or several contemporaneous or
536 successive stages processes in order to explain the dunite trace element signatures. It is worth
537 mentioning that the single- and two-stages processes were proposed in order to mimic
538 harzburgite signatures (Navon and Stolper, 1987; Godard et al., 1995; Vernières et al., 1997),
539 but it may be different for dunites.
540
541 As the trace element enrichment in pure dunites relative to harzburgites cannot be accounted
542 for by V1-type (e.g. Godard et al., 2003) MORB percolation alone, it therefore calls for the
543 additional involvement of a more enriched melt. In the same spirit Godard et al. (2000)
544 proposed the pervasive infiltration of volatile- and LILE-enriched small melt fractions to
545 account for the enrichment in Th, Nb and Ta relative to LREE in mantle harzburgites. The
546 interaction between an incompatible trace elements-enriched melt or fluid and the
547 surrounding dunites does not contradict the percolation of MORB through the DTZ, and the
548 migration of different kinds of melt is further supported by the variable composition of
549 clinopyroxenes located in interstitial position between olivine grains (Fig. 6) (see also Koga et

al., 2001) and by the presence of amphibole and orthopyroxene among other which are not expected in the fractionation path of primitive MORB (Rospabé et al., 2017). Furthermore, two strong arguments in favour to MORB percolation through the DTZ are the particularly high CaO content in olivine especially observed in pure dunites (Fig. 4b), consistent with MORB-dunite equilibration before cooling (Abily and Ceuleneer, 2013), and the high TiO_2 content in disseminated chromites and impregnant pyroxenes (Fig. 4e and f) (see also Rospabé et al., 2017). In a profile view along the base (pure dunites) of the Buri cross section (Fig. 1b), chemical evolutions from about 640 m to 700 m high show that high CaO values in olivine are strongly correlated to other chemical species (Fig. 8), independently from the very small amount of interstitial clinopyroxene (Table 1). This includes high Gd_{CN}/Yb_{CN} ratio in whole rock (Gd increases from 2.5 to 9.5 ng/g respectively) and a higher concavity of the REE patterns (i.e. well-defined U-/V-shaped REE patterns), but also higher Co content in whole rock and TiO_2 content both in chromite and scarce minute clinopyroxenes. On the contrary, the 700 m level is characterized by lower Fo in olivine (and Ni content both in olivine and whole rock) and La_{CN}/Sm_{CN} ratio in whole rock (faster increase of Sm (from 4.8 to 7.8 ng/g) relative to La (from 1.1 to 5.0 ng/g)). Assuming that high CaO in olivine recorded the last re-equilibration with a percolating MORB before cooling (Abily and Ceuleneer, 2013), these co-evolutions highlight that dunites had overprinted a prior enrichment in LREE and a strong concave-upward REE pattern signature before the accumulation and the re-equilibration with MORB at 700 m followed by the compaction of the dunitic matrix.

These observations have several major implications: (1) considering that such enrichments in incompatible elements may be attributable to a low melt-rock ratio (i.e. low porosity) and/or to chromatographic effects induced by the migration of a highly enriched melt (Navon and Stolper, 1987; Godard et al., 1995; Vernières et al., 1997), the low CaO in olivine for the most

LREE-enriched samples better supports the re-equilibration with an incompatible elements-rich melt or fluid early in the magmatic history of the DTZ; (2) dunites displaying the highest La_{CN}/Sm_{CN} ratios do not represent an end-member that was percolated by a higher amount of melt (Navon and Stolper, 1987) but result from the more or less significant interaction with this early enriched melt or fluid; (3) the percolation of MORB-type melts did not occur all over the DTZ and seems to have been focused at some particular horizons at an advanced stage of the DTZ structuration (i.e. here the 700 m high level); (4) the increase of the La, Sm and Gd contents until 700 m implies that the re-equilibration with MORB indeed enhanced the enrichment in the most incompatible LREE, but mostly affected and re-enriched the dunitic matrix in the previously most depleted MREE. Especially, from the base to the elevation of 700 m along the Buri cross section, the faster increase of Gd_{CN}/Dy_{CN} (0.33 to 0.53) relative to Er_{CN}/Yb_{CN} (0.47 to 0.53) follows the smoothing of MREE-HREE segment pattern. In this way the linear REE patterns in dunites and harzburgites have been interpreted as resulting from re-equilibration induced by MORB-type melt transport (Godard et al., 2000), while concave-upward patterns observed through the DTZ and in mantle harzburgites from the Maqsad area should be better related to the dunitization process. Therefore, MORB percolation led to a decrease of the LREE/MREE and an increase and MREE/HREE ratios, and to smoother REE patterns (i.e. exhibiting a lower concavity). Accordingly, dunites from the DTZ appear to be generated after a multi-stages process: (1) a complete harzburgite reactional melting during which enriched melt batches are generated probably in low volume (i.e. melt generated by the incongruent melting of orthopyroxene associated with the contribution of fluids and minor amount of MORB) followed by (2) a chemical re-equilibration with larger amount of percolating MORB. In opposition with the model of Navon and Stolper (1987), we propose that the incompatible trace elements-enriched signature is a feature acquired early during the dunitization rather than later by the percolation

of enriched melts.

6.3.3. About the habitus of incompatible trace elements in the dunitic matrix

As previously discussed, the trace element enrichment in dunite, especially in LREE, may better reflect magmatic processes rather than secondary alteration events (paragraph 6.1). It supports the view that trace elements are hosted by the olivine itself rather than by interstitial serpentine surrounding preserved grains and is in accordance with recent trace element data in olivine obtained by laser ablation methods (e.g. Drouin et al., 2009; Rampone et al., 2016; Stead et al., 2017). Sub-solidus re-equilibration between olivine and other mineral phases may eventually occur (Sun and Liang, 2014) and lead to trace element enrichments at olivine grains boundary (Stead et al., 2017), while other studies propose that these particular geochemical signatures reflect analytical artefacts or the entrapment of small LREE-rich melt inclusions (e.g. Lee et al., 2007). The analytical method we developed (Rospabé et al., 2018) allowed us to establish with confidence that the extensive enrichment in LREE relative to MREE in pure dunites (Fig. 5) is a reliable result. These enrichments thus cannot be satisfactorily explained both by analytical effects or re-equilibration with other minerals. Furthermore, we did not detect melt inclusions through microscopic observations and during the electron microprobe sessions, although the existence of inclusions smaller than about 10 µm cannot be excluded. Finally, the absence of zoning in olivine grains, at least in terms of major elements, does not militate for a possible concentration of incompatible elements at grain boundaries. All these observations support the hosting of the incompatible trace elements by crystal lattices in olivine consecutively to re-equilibration of the olivine matrix with interstitial melts during their migration through the DTZ. Sub-solidus re-equilibration between different olivine grains may lead to the trace element content smoothing between rims and cores, but stays a hypothetical track at this stage and should be explored in future

625 works.

626

627 *6.4. Refertilization induced by melt transport*

628 Interstitial minerals in impregnated dunites may be considered as crystallization products
629 from a melt percolating through the residual and porous dunitic media (e.g. Benn et al., 1988;
630 Rabinowicz et al., 1987; Kelemen et al., 1995a; Boudier and Nicolas, 1995; Koga et al.,
631 2001), rather than as trapped melts not perfectly extracted (e.g. Faul, 1997; Sundberg et al.,
632 2010). This reasonable assumption is supported by the systematic high Mg# in pyroxenes and
633 generally high An in plagioclases, as well as by the low REE contents both in clinopyroxenes
634 and whole rocks, that are all together not expected in the case of MORB-like melt entrapment
635 between olivine grains (see also Koga et al., 2001). Basically, the whole impregnated dunite
636 composition is strongly impacted by the modal abundance of these interstitial minerals,
637 especially by the amount of clinopyroxene (Fig. 5 and Appendix C).

638

639 *6.4.1. Diversity of the percolating melts within the Maqsad DTZ*

640 Calculated melts in equilibrium with clinopyroxenes impregnating the DTZ appear much
641 more variable than the melts that migrated through the mantle section (Benoit et al., 1996;
642 Benoit, 1997) and the V1 lavas constituting the upper crust in the Sumail massif (Godard et
643 al., 2003) (Fig. 9). Three main types of patterns are observed: clinopyroxenes in equilibrium
644 with (1) a N-MORB type melt (1 sample of cpx-bearing dunite) (Fig. 9a), (2) LREE-enriched
645 melts (mainly in (pl/)cpx-bearing dunites) (Fig. 9b), (3) strongly LREE-depleted melts
646 (mainly in (amph/)opx/pl/cpx-bearing dunites) (Fig. 9c). HREE melt concentrations are
647 basically in the variation range of the MORB-type (or V1, Godard et al., 2003) lavas but are
648 much more variable in LREE. The presence of minerals supposed to be in equilibrium with
649 both LREE-enriched and LREE-depleted melts through the DTZ may reflect either the mixing

between various melt batches, including a high proportion of deep melts issued from low mantle partial melting degrees, or the reaction at shallow depth between a primitive MORB and residual depleted peridotites (Sobolev, 1996; Kelemen et al., 1997b; Koga et al., 2001). The first hypothesis would seem unlikely here since the absence of such derived enriched-like cumulates in the mantle section. Indeed, MORB-parent melts that crystallized primitive troctolite sills cropping out in the Maqsad harzburgites show quite geochemical variations attributable to different degrees of partial melting within the diapir (Benoit, 1997), but that are much more restricted than the melt diversity described here.

6.4.2. Early generation of enriched melt batches during dunitization

The Maqsad area is characterized by the absence of cumulates crystallized from an enriched parent melt within both the mantle section and the DTZ (Benoit et al., 1996; Kelemen et al., 1997a; Python and Ceuleneer, 2013). According to this and to the trace element enrichments in pure dunites (Fig. 5), we propose the early production of LREE-enriched melts at Moho level (Fig. 9b) further related to melt-rock reactions rather than originated from depth. These melts can be related to the SiO_2-enriched melts produced during incongruent melting of the orthopyroxene and expected following the study of other ophiolitic massifs (Dick, 1977; Quick, 1981; Kelemen, 1990; Kelemen et al., 1992). The early involvement of an enriched melt responsible of the incompatible trace element enrichment in olivine, deduced from the whole pure dunite composition, is in accordance with this interpretation.

The genesis of highly enriched melts during dunitization, and the incipient crystallization, may be related to reactive crystallization (Collier and Kelemen, 2010). This process was identified as the main cause of clinopyroxene chemical zoning in olivine-rich troctolites from slow spreading environments: cores were generated by fractional crystallization from a

675 percolating melt while enriched rims result from the fractionation after the contamination of
676 the melt by assimilation of the surrounding peridotite (e.g. Suhr et al., 2008; Drouin et al.,
677 2009; Sanfilippo et al., 2013, 2015; Rampone et al., 2016). Especially, the resorption of
678 orthopyroxene seems to be a credible source for this particular signature, allowing to
679 important Zr_{CN}/Nd_{CN} fractionation (until 1.5) with the increase of REE contents (Sanfilippo et
680 al., 2015). In this way, the dunitization, when directly followed by interstitial mineral
681 fractionation, can be presented as a kind of reactive crystallization process considering the
682 enrichment in silica and incompatible trace elements of the residual melt. However, in this
683 study, clinopyroxene grains analyzed for their trace elements are not zoned and present low
684 Zr_{CN}/Nd_{CN} ratios (0.34-0.74; 0.47 in average) with no observed correlation with Yb, similar to
685 clinopyroxene cores in olivine-rich troctolites. This highlights that the chemical evolution of
686 enriched melt batches is probably, in the frame of the Maqsad DTZ, firstly dominated by the
687 residual orthopyroxene assimilation process by MORB (i.e. reactive crystallization in the case
688 of clinopyroxene fractionation at this stage). Following the complete orthopyroxene
689 resorption, fractional crystallization occurs while MORB issued from partial melting within
690 the Maqsad diapir are introduced and transferred through the porous olivine matrix without
691 any further reaction.
692
693 *6.4.3. Differentiation and hybridization of the percolating melts within the Maqsad DTZ*
694 Oppositely, further hypotheses may be proposed concerning the LREE-depleted melts (Fig.
695 9c), which may reflect (1) the assimilation of the surrounding dunite at an advanced
696 refertilization stage (i.e. reactive crystallization products), (2) the later sub-solidus re-
697 equilibration between clinopyroxene crystals and neighbouring mineral phases (e.g. Sun and
698 Liang, 2014), (3) the result of hybridization between a latter percolating MORB and hydrous
699 fluids (Rospabé et al. 2017). The two first hypotheses difficultly account for the large

chemical variations in clinopyroxene, that is the most common and abundant impregnant phase in DTZ dunites, especially concerning the variable slope of the HREE segment (Figs. 6 and 9). However, the third hypothesis is supported by the fact that the LREE-depleted signature is observed mainly in samples containing interstitial orthopyroxene and/or amphibole, minerals previously interpreted as fractionated from a hybrid melt between MORB and hydrous fluids (Rospabé et al., 2017). In this scenario this hybrid component may contribute to the exotic melt involved in the formation of disseminated chromites and chromitite ore bodies as suggested by the numerous inclusions of hydrous minerals in chromite (Lorand et Ceuleneer, 1989; Leblanc et Ceuleneer, 1991; Borisova et al., 2012; Rospabé et al., 2017; Johan et al., 2017).

To conclude, our study reveals that the variability in the composition of the melts responsible of the dunite formation and of their petrological and geochemical evolution is extremely pronounced (see also Sanfilippo et al., 2014, 2017). A working hypothesis is to consider that such wide melt variability is a specificity of the DTZ and reflects local melt/fluid-rock reactions rather than a complex mixing of deep-seated melt batches. This assumption is supported by the fact that some clinopyroxene grains exhibiting different patterns were analysed in samples collected in nearly same locations (Table 1 and Appendix B). According to the observed clinopyroxene chemical heterogeneity, it appears that the DTZ evolved as an open reactive system in which melts fractions issued from strong melt-rock interactions evolved by fractional crystallization and hybridization and were far from being fully homogenised before being supplied to the lower crust.

6.5. Synthetic model for the formation of the Maqsad DTZ

As pointed out here above, none of the four main processes that are discussed - (1)

725 serpentinization or secondary weathering, (2) fractionation and accumulation of olivine, (3)
726 harzburgite reactional melting and re-equilibration related to melt percolation into dunite
727 porosity, and (4) refertilization through minerals crystallization from percolating melts
728 interstitially between olivine grains - may account alone for the wide spectrum of
729 geochemical signatures observed in whole rock and mineral compositions of the DTZ,
730 although each can contribute to account for part of this variability, depending on the elements
731 considered. This indicates that the DTZ records an overprinting of several processes.
732
733 In attempt to propose a general scenario describing the development of the Maqsad DTZ,
734 Figure 10 summarizes the different steps deduced from the whole rock and mineral major and
735 trace element signatures. The starting lithology, i.e. the harzburgite from the specific Maqsad
736 area, present a slight but significant LREE enrichment relative to the harzburgites from the
737 main mantle section located far away from the diapir (Fig. 10a) (Godard et al., 2000). Acting
738 as a filter for ascending melts, the top of the diapir is progressively transformed into dunites
739 by interaction with interstitial melts, probably of MORB affinity (Fig. 10b). This process
740 leads to the depletion in HREE in the residual dunite due to the resorption of the last
741 pyroxenes and to the enrichment in LREE and other incompatible trace elements (HFSE, Th,
742 U and possibly some LILE as Rb and Ba). This signature is better explained by the early
743 generation of small batches of enriched melts in response to orthopyroxene incongruent
744 melting (i.e. enriched residual melt). At start, the reaction is driven by MORB/harzburgite
745 interaction but the olivine matrix records the solely incompatible trace elements enrichment,
746 calling for a very low porosity needed to preserve this signature. It has been proposed that
747 high temperature hydrothermal fluids were involved in dunite formation or as early as the
748 mantle dunitization process (Bowen and Tuttle, 1949; Rospabé et al., 2017; Johan et al.,
749 2017); the enriched signature described in this paper may be another evidence for the early

750 hydration of the DTZ. Following this, the dunitization will increase the permeability, as
751 MORB-like melts delivered by the mantle continue to invade the matrix. Those melts no
752 longer contribute to mineralogical reaction following the complete orthopyroxene resorption
753 within the host rock, and then may accumulate at Moho level or feed the crust (Fig. 10c and
754 10d). Chemical re-equilibration occurs during MORB percolation, leading to a slight LREE
755 and mainly MREE enrichment in the host dunite, i.e. the re-equilibration process seems to
756 mainly affect the most depleted trace elements in the dunitic matrix independently from the
757 partition coefficient between those elements and olivine. The chemical overprinting of this
758 stage occurs until the compaction of the matrix and the resulting melt extraction. It is worth
759 mentioning that all the intermediate cases may exist between a pure dunite having preserved
760 its prior enriched signature (Fig. 10e) and another one having been fully re-equilibrated with
761 MORB (Fig. 10f). Therefore, pure dunites may be considered as a witness of a magmatic
762 system closed at very high temperature (i.e. above the olivine-plagioclase-clinopyroxene
763 ternary cotectic). Depending on the thermal state of the DTZ, and certainly on the primitive or
764 evolved nature of the percolating melt, crystallization will or not occur interstitially. As
765 supposed following the various REE patterns calculated for the olivine matrix hosting some
766 impregnating clinopyroxene (Appendix C), mineral fractionation occurs concomitantly with
767 the melt percolation and re-equilibration processes (Fig. 10g). Among other, the circulation of
768 hydrous fluids at Moho level during the structuration of the DTZ explains: (1) the higher
769 amount of impregnations approaching the base of the crust witnessing the former thermal
770 gradient across DTZ (Rospabé et al., 2017; see also Dygert et al., 2017), (2) the harzburgite
771 dunitization in the specific context of the DTZ, and not to deeper dunite channels within the
772 mantle section, and (3) the interstitial mineralogy indicative of the percolation of exotic
773 hybrid melts certainly involved in the transport of high amount of Cr - potentially released
774 from orthopyroxene during the dunitization (Johan et al., 2017) - and its concentration in

775 disseminated chromites and chromitite pods (Rospabé et al., 2017). In the case of a much
776 colder environment as in slower-spreading environment (Collier and Kelemen, 2010),
777 extreme refertilization potentially occur through a more efficient assimilation of the olivine
778 matrix coupled to fractional crystallization (reactive crystallization), leading to the formation
779 of olivine-rich troctolites as observed in samples collected along present-day mid-ocean
780 ridges or within ophiolites DTZ (e.g. Suhr et al., 2008; Drouin et al., 2009; Dick et al., 2010;
781 Sanfilippo and Tribuzio, 2013b; Sanfilippo et al., 2013, 2014, 2015; Rampone et al., 2016).
782 At this stage, it cannot be excluded that the fractional crystallization dominated the
783 refertilization process within the Maqsad DTZ, relative to reactive crystallization, due to the
784 fast spreading environment in which the Oman ophiolite likely evolved. Another possibility
785 consists in the fast cooling of this oceanic lithosphere fragment, related to the oceanic
786 thrusting that directly followed the lithosphere accretion and that fossilized the system in a
787 high temperature configuration (Boudier et al., 1988). Finally, in regard to the whole dunites
788 and mineral major and trace elements, it appears that both pure and variably impregnated
789 dunites represent end-members that can be generated independently.
790
791 As shown, the re-equilibration with percolating MORB did not occur equally all along the
792 DTZ but was more efficient at some specific levels (Fig. 8) (see also Abily and Ceuleneer,
793 2013), suggesting that the dunitic matrix was either unequally compacted when MORB
794 migrated through it or that the MORB percolation was locally focused. This feature may be
795 partially explained by a model of progressive downward dunitization of the mantle
796 harzburgites at the top of the Maqsad diapir (Abily and Ceuleneer, 2013). During this process,
797 the compaction may progress downward, possibly in response from cooling from above,
798 through successive steps and then may spatially constrain the porous fronts in which MORB
799 may have accumulated. Clearly, some horizons of the DTZ remained isolated early after

dunitization and other horizons were intensely re-equilibrated with MORB more or less hybridized with hydrous, likely hydrothermal fluids.

7. Conclusion

Major and trace elements of 79 pure to highly impregnated dunites from the Oman ophiolite and the composition of the impregnation minerals revealed a large petrological and chemical variability. The dunitic matrix - measured pure dunites and modelled olivine matrix in impregnated dunites - is characterized by a more or less pronounced concave-upward REE pattern and a variable enrichment in other incompatible HFSE, Th, U, Rb and Ba. Their REE and multi-elements patterns are highly scattered implying that no dominant single process controlled the dunite formation. Chemical evolutions suggest that the enriched signature was recorded early during the dunitization by interaction between the surrounding olivine matrix and incompatible trace elements-rich small melt batches at low melt/rock ratios. The latest MORB percolation leads to a cryptic metasomatism expressed as smoothest REE patterns, among others, inducing flattest slopes in HREE and LREE patterns. This scenario contradicts the later percolation of a deep-seated enriched melt and better supports that hybrid enriched melts are generated by melt/rock reactions at an early magmatic stage within the DTZ beneath mid-ocean spreading centers.

Our survey shows that these different signatures are variably distributed along the DTZ. This implies that some horizons have been compacted early immediately following the mantle harzburgites dunitization, while others maintained a high enough permeability to drain MORB and make possible re-equilibration. The physical processes that condition the heterogeneous chemical distribution along the DTZ remains quite enigmatic at this stage. Pure and impregnated dunites may be considered as two lithological end-members starting

825 from a common dunitized peridotitic matrix: the first have been compacted at very high
826 temperature after various chemical re-equilibration degrees and the complete extraction of
827 interstitial percolating melts, while the others have been modally refertilized before the
828 extraction of the residual melt. In this frame, the combination of whole dunites and *in situ*
829 minerals major and trace elements compositions reveals undoubtedly the multi-stages
830 processes involved in the DTZ generation.
831
832 Finally, based on the chemical variability within the different minerals observed in dunites
833 from the DTZ, we conclude that if MORB magmas generated by mantle partial melting may
834 have been partly homogenized within the uppermost mantle before being supplied to the
835 mantle-crust transition zone, melt-rock reactions and hybridization processes occurring within
836 the DTZ may generate new, exotic and/or hybrid, melt batches that will participate to the
837 oceanic crust genesis and potentially to the MORB heterogeneity. The precise relationship
838 between the evolution of the Maqsad diapir, the N130 paleo-ridge axis, and the vertical
839 petrological and geochemical signatures across the DTZ is a complex three-dimensional
840 problem and could be deciphered by a more comprehensive structural, petrological and
841 geochemical survey of the area.
842
843 **Acknowledgments**
844 We are grateful to F. de Parseval, J.-F. Ména and L. Menjot for thin sections preparation, S.
845 Gouy, J. Langlade and P. de Parseval for technical assistance during microprobe analysis, and
846 to F. Candaudap and D. Roggero for technical assistance during whole rock trace elements
847 analysis by HR-ICP-MS and clinopyroxene trace elements acquisition by laser ablation (LA-
848 ICP-MS) respectively. Y. Liang, T. Morishita and A. Sanfilippo are thanked for their highly
849 constructive comments that helped to improve the paper. Informal discussions with and

questions/comments from N. Dygert were also greatly appreciated. This work has benefited from a financial support provided by the Centre National de la Recherche Scientifique-Institut National des Sciences de l'Univers (CNRS-INSU). M.-A. Kaczmarek thanks the Swiss National Science Foundation (SNSF) for support from Ambizione grants PZ00P2_142454 and PZ00P2_166933. For their hospitality and assistance H. Al Azri as well as M. Al Araimi, M. Al Batashi, A. Al-Rajhi and other people from the Ministry of Commerce and Industry, Sultanate of Oman, are greatly acknowledged.

Figure 1. Geological map of the Oman ophiolite showing (1) the spatial distribution of the mantle and crustal sections and (2) the two main magmatic suites displayed along the ophiolite regarding the nature of the dikes cross-cutting the mantle section, characterized as the depleted-andesitic series and the and N-MORB tholeiitic one (a). The Sumail massif exposes a dunitic transition zone of about 300 m thick above the Maqsad mantle diapir (b). Four cross sections were sampled in this area.

Figure 2. Photomicrographs illustrating the mineralogical diversity that allowed to define the different lithological facies observed within the Oman ophiolite DTZ, with the olivines constituting the matrix of a pure dunite (a), the comparison between a well developed impregnant clinopyroxene oikocryst in a cpx-bearing dunite (b) with a small interstitial diopside in a pure dunite (c), a plagioclase oïkocryst in a pl/cpx-bearing dunite (d), an orthopyroxene oikocryst in a opx/pl/cpx-bearing dunite (e), and an amphibole in a amphibole-bearing dunite.

Figure 3. Whole rock major and minor element compositions of the studied dunites in the Maqsad dunites (coloured circles) compared to other DTZ dunites (open circles), mantle

harzburgites (open squares) and cpx-harzburgites/lherzolites (open diamonds) from the Oman ophiolite (Godard et al., 2000; Gerbert-Gaillard, 2002; Takazawa et al., 2003; Monnier et al., 2006; Hanghøj et al., 2010; Khedr et al., 2014; Nicolle et al., 2016). (a) MgO/SiO_2 versus Al_2O_3/SiO_2, (b) total iron as FeO versus MgO, (c) Al_2O_3 versus CaO, and (d) Ni and (e) Co as a function of the Mg# ratio (100 × molar $Mg/(Mg + Fe_{total})$). Compositions are recalculated on a volatile-free basis. Grey bar in panel (a) represents the silicate Earth differentiation trend (or "terrestrial array") (Jagoutz et al., 1979). Dashed black line in panel (b) represents the variation of olivine composition constrained by FeO + MgO = 66.67 mol% following Godard et al. (2000). Dashed grey lines in panels (b) and (c) represent constant Mg# and Al_2O_3/CaO ratios respectively.

Figure 4. Mineral major element compositions of the studied dunites from the Maqsad area illustrated in (a) NiO in olivine, (b) CaO in olivine and (c) Mg# in whole rock as a function of Fo in olivine, in (d) Cr# (100 × molar Cr/(Cr + Al) in chromite versus Fo in olivine with the olivine-spinel mantle array (OSMA) from (Arai, 1987; Arai, 1994) (grey field), (e) TiO_2 versus Mg# ratio (100 × molar $Mg/(Mg + Fe^{2+})$ in chromite and (f) TiO_2 as a function of Mg# ratio (100 × molar $Mg/(Mg + Fe^{2+})$ in clinopyroxene. Dark blue dots in clinopyroxene plots are the small diopsides observed at olivine grains rims in both pure and impregnated dunites. They are plotted whatever their hosting lithological facies, displaying a composition range spanning between igneous clinopyroxenes and pure hydrothermal diopsides (Rospabé et al., 2017).

Figure 5. Whole rock chondrite-normalized REE (a, c, e and g) and Primitive Mantle-normalized multi-elements (b, b, f and h) patterns of the studied dunites from the Maqsad dunitic transition zone. Colour labels following the figure 2 for pure dunites (a and b), cpx-

bearing dunites (c and d), pl/cpx-bearing dunites (e and f), and opx/pl/cpx-bearing dunites and amphibole-bearing dunites (±opx, pl and cpx) (g and h). In the panels (a) and (b) pure dunites patterns (blue lines) are compared to the harzburgites from the whole Oman ophiolite mantle section (white field framed with a dashed black line) (Gerbert-Gaillard, 2002; Takazawa et al., 2003; Monnier et al., 2006; Hanghøj et al., 2010; Khedr et al., 2014; Nicolle et al., 2016) and to the main mantle harzburgites from the Sumail massif (light grey field), the harzburgites from the Maqsad diapir area (medium grey field) and few other dunites from the Maqsad DTZ (dark grey field) (Godard et al., 2000; Gerbert-Gaillard, 2002). In other panels each lithological facies is compared to the field of pure dunites from this study (blue fields). Normalizing chondrite and Primitive Mantle values are from Barrat et al. (2012) and Sun and McDonough (1989) respectively.

Figure 6. Clinopyroxene chondrite-normalized REE (a) and Primitive Mantle-normalized multi-elements patterns (b). Normalizing chondrite and Primitive Mantle values are from Barrat et al. (2012) and Sun and McDonough (1989) respectively.

Figure 7. Trace element co-evolutions in pure dunites represented as (a) La, (b) U, (c) Zr, (d) Ta, (e) Rb and (f) Ba as a function of Th.

Figure 8. Chemical evolutions along the base of the Buri cross section, made of pure dunites, illustrated in Fo and NiO in olivine, and whole rock La_{CN}/Sm_{CN} and Gd_{CN}/Yb_{CN} ratios as well as the degree of concavity of their REE patterns, all as a function of the absolute elevation of the sampling site. The concavity of the REE patterns was calculated for each sample as $[\sqrt{(Sm_{CN} \times Gd_{CN})}/\sqrt{(Ce_{CN} \times Yb_{CN})} -1]$. All these co-evolutions are a further strong evidence for the hosting of incompatible trace elements by olivine itself.

925

926 **Figure 9.** Calculated equilibrium melts with the interstitial clinopyroxenes in impregnated
927 dunites from the Maqsad DTZ. Clinopyroxene compositions were averaged for each sample
928 to perform the calculation. Compositions are presented following the shape of the REE
929 patterns with (a) MORB-type melts, (b) LREE-enriched melts and (c) LREE-depleted melts.
930 Calculated melts are compared to the Oman ophiolite V1 (red field) and V2 (green fields)
931 lavas (Godard et al., 2003; Godard et al., 2006) and boninites (dark green field) (Ishikawa et
932 al., 2002; Ishikawa et al., 2005). N-MORB values are from Sun and McDonough (1989).
933 Partitioning coefficients used in the calculation are from Bédard (1994) and normalizing
934 chondrite values are from Barrat et al. (2012). It is worth mentioning that clinopyroxene is the
935 most abundant impregnating phase, and is supposed to display the higher trace element
936 contents in dunites, together with amphibole. In regard of the large HREE content variations
937 in clinopyroxene, it is difficult to account for this variability following sub-solidus re-
938 equilibration with other minerals present (e.g. Sun and Liang, 2014), especially in the
939 restricted temperature range expected with the cotectique ol-pl-cpx. Thus it is assumed that
940 re-equilibration between clinopyroxene and neighbouring olivine, orthopyroxene, plagioclase
941 and/or amphibole is negligible as far as the REE are concerned (i.e. the assumption of a low
942 REE diffusivity at subsolidus temperature following Van Orman et al., 2001). Then, the
943 calculation of the inferred melt in equilibrium from which the clinopyroxene crystallized
944 allows investigating the nature of the melt that percolated and fractionated interstitial minerals
945 through dunitic rocks.

946

947 **Figure 10.** Synthetic model for the genesis of the dunites from the Maqsad DTZ,
948 summarizing the melt-rock reactions leading to their high petrological and geochemical
949 variability: (a) incongruent melting of orthopyroxene in mantle harzburgites just below Moho

level, (b) neo-formed dunite comprising interstitial high-silica and trace elements-enriched small melt batches, (c) MORB infiltration within the porosity, leading to a hybridization process between the former enriched melt and the incoming MORB, and (d) intense migration of variably evolved MORB batches, leading to variably extensive chemical re-equilibration with the surrounding dunitic matrix. Pure dunites may be produced at different stages over the successive melt-rock reactions, directly following the dunites genesis when they are enriched in the most incompatible elements as LREE (U-shaped REE pattern as the blue line) (e), or after strong re-equilibration with the percolating MORB that allowed to the enrichment in MREE in the olivine matrix (i.e. smoothing of the REE pattern) (f). The chemical signature of pure dunites will first depend on the amount of melt that percolated and re-equilibrated with the host dunites and second on the chemistry of this melt. In some cases, mineral crystallization occurs through the DTZ leading to the formation of impregnated dunites after extraction of the residual melt and compaction of the matrix (g). Refertilization may occur at any moment of the evolution of the system, either within a neo-formed dunite or within a fully re-equilibrated one after intense MORB percolation. In that case the whole rock chemical signature will depend on (1) the composition of the olivine matrix, (2) the amount of fractionated minerals interstitially and (3) the composition of these minerals.

Table 1. Location and modal composition of the samples analysed in this study. The modal abundance of each mineral was calculated using both whole rock and mineral major elements. Mode calculations were systematically compared to and are in good agreement with thin section observations.

Appendix A. Whole rock major and trace element compositions.

975 **Appendix B.** Mineral major element compositions and clinopyroxene trace element
976 compositions.
977
978 **Appendix C.** Modelling of the interstitial minerals modal abundance influence on the whole
979 rock chemical content
980
981 **References**

982 Abily B. and Ceuleneer G. (2013) The dunitic mantle-crust transition zone in the Oman
983 ophiolite: Residue of melt-rock interaction, cumulates from high-MgO melts, or both?
984 *Geology* **41**, 67-70.
985 Akizawa N., Ozawa K., Tamura A., Michibayashi K. and Arai S. (2016a) Three-dimensional
986 evolution of melting, heat and melt transfer in ascending mantle beneath a fast-spreading
987 ridge segment constrained by trace elements in clinopyroxene from concordant dunites
988 and host harzburgites of the Oman ophiolite. *J*. *Petrol*. **57**, 777-814.
989 Akizawa N., Tamura A., Fukushi K., Yamamoto J., Mizukami T., Python M. and Arai S.
990 (2016b) High-temperature hydrothermal activities around suboceanic Moho: An example
991 from diopsidite and anorthosite in Wadi Fizh, Oman ophiolite. *Lithos* **263**, 66-87.
992 Arai S. (1987) An estimation of the least depleted spinel peridotite on the basis of olivine-
993 spinel mantle array. *Neues Jahrb*. *für Mineral*. - *Monatshefte* **8**, 347-354.
994 Arai S. (1994) Characterization of spinel peridotites by olivine-spinel compositional
995 relationships: Review and interpretation. *Chem*. *Geol*. **113**, 191-204.
996 Arai S. and Matsukage K. (1996) Petrology of gabbro-troctolite-peridotite complex from Hess
997 Deep, equatorial Pacific: implications for mantle-melt interaction within the oceanic
998 lithosphere. *Proc*. *Ocean Drill*. *Program, Sci*. *Results* **147**, 135-155.
999 Bach W., Garrido C. J., Paulick H., Harvey J. and Rosner M. (2004) Seawater-peridotite

1000 interactions: First insights from ODP Leg 209, MAR 15°N. *Geochemistry, Geophys*.
1001 *Geosystems* **5**.
1002 Barrat J.-A., Keller F., Amossé J., Taylor R. n., Nesbitt R. w. and Hirata T. (1996)
1003 Determination of Rare Earth Elements in Sixteen Silicate Reference Samples by Icp-Ms
1004 After Tm Addition and Ion Exchange Separation. *Geostand*. *Newsl*. **20**, 133-139.
1005 Barrat J.-A., Zanda B., Moynier F., Bollinger C., Liorzou C. and Bayon G. (2012)
1006 Geochemistry of CI chondrites: Major and trace elements, and Cu and Zn Isotopes.
1007 *Geochim*. *Cosmochim*. *Acta* **83**, 79-92.
1008 Bédard J. H. (1994) A procedure for calculating the equilibrium distribution of trace elements
1009 among the minerals of cumulate rocks, and the concentration of trace elements in the
1010 coexisting liquids. *Chem*. *Geol*. **118**, 143-153.
1011 Bédard J. H. and Hébert R. (1998) Formation of chromitites by assimilation of crustal
1012 pyroxenites and gabbros into peridotitic intrusions: North Arm Mountain massif, Bay of
1013 Islands ophiolite, Newfoundland, Canada. *J*. *Geophys*. *Res*. *Earth* **103**, 5165-5184.
1014 Benn K., Nicolas A. and Reuber I. (1988) Mantle-crust transition zone and origin of wehrlitic
1015 magmas: Evidence from the Oman ophiolite. *Tectonophysics* **151**, 75-85.
1016 Benoit M. (1997) Caractérisation géochimique (traces, isotopes) d'un système de drainage
1017 magmatique fossile dans l'ophiolite d'Oman. *PhD thesis* Université Toulouse III - Paul
1018 Sabatier, 257 pp.
1019 Benoit M., Ceuleneer G. and Polvé M. (1999) The remelting of hydrothermally altered
1020 peridotite at mid-ocean ridges by intruding mantle diapirs. *Nature* **402**, 514-518.
1021 Benoit M., Polvé M. and Ceuleneer G. (1996) Trace element and isotopic characterization of
1022 mafic cumulates in a fossil mantle diapir (Oman ophiolite). *Chem*. *Geol*. **134**, 199-214.
1023 Berger E. T. and Vannier M. (1984) Les dunites en enclaves dans les basaltes alcalins des iles
1024 oceaniques: approche petrologique. *Bull*. *Mineral*. **107**, 649-663.

1025 Bodinier J. L., Vasseur G., Vernières J., Dupuy C. and Fabries J. (1990) Mechanisms of
1026 Mantle Metasomatism: Geochemical Evidence from the Lherz Orogenic Peridotite. *J*.
1027 *Petrol*. **31**, 597-628.
1028 Borisova A. Y., Ceuleneer G., Kamenetsky V. S., Arai S., Béjina F., Abily B., Bindeman I.
1029 N., Polvé M., De parseval P., Aigouy T. and Pokrovski G. S. (2012) A new view on the
1030 petrogenesis of the Oman ophiolite chromitites from microanalyses of chromite-hosted
1031 inclusions. *J*. *Petrol*. **53**, 2411-2440.
1032 Boschi C., Dini A., Früh-Green G. L. and Kelley D. S. (2008) Isotopic and element exchange
1033 during serpentinization and metasomatism at the Atlantis Massif (MAR 30°N): Insights
1034 from B and Sr isotope data. *Geochim*. *Cosmochim*. *Acta* **72**, 1801-1823.
1035 Boudier F., Bouchez J. L., Nicolas A., Cannat M., Ceuleneer G., Misseri M. and Montigny R.
1036 (1985) Kinematics of oceanic thrusting in the Oman ophiolite: model of plate
1037 convergence. *Earth Planet*. *Sci*. *Lett*. **75**, 215-222.
1038 Boudier F., Ceuleneer G. and Nicolas A. (1988) Shear zones, thrusts and related magmatism
1039 in the Oman ophiolite: Initiation of thrusting on an oceanic ridge. *Tectonophysics* **151**,
1040 275-296.
1041 Boudier F. and Coleman R. G. (1981) Cross section through the peridotite in the Samail
1042 Ophiolite, southeastern Oman Mountains. *J*. *Geophys*. *Res*. *Solid Earth* **86**, 2573-2592.
1043 Boudier F. and Nicolas A. (1995) Nature of the moho transition zone in the Oman ophiolite.
1044 *J*. *Petrol*. **36**, 777-796.
1045 Bouilhol P., Burg J. P., Bodinier J. L., Schmidt M. W., Dawood H. and Hussain S. (2009)
1046 Magma and fluid percolation in arc to forearc mantle: Evidence from Sapat (Kohistan,
1047 Northern Pakistan). *Lithos* **107**, 17-37.
1048 Bowen N. L. (1915) The later stages of the evolution of the igneous rocks. *J*. *Geol*. **23**, 1–91.
1049 Bowen N. L. (1927) The Origin of ultra-basic and related rocks. *Am*. *J*. *Sci*. **14**, 89-108.

1050 Bowen N. L. and Tuttle O. F. (1949) The System MgO-SiO_2-H_2O. *Geol*. *Soc*. *Am*. *Bull*. **60**,
1051 439.
1052 Ceuleneer G. (1986) Structure des ophiolites d'Oman : flux mantellaire sous un centre
1053 d'expansion océanique et charriage à la dorsale. *PhD thesis* Université de Nantes, 349
1054 pp.
1055 Ceuleneer G. (1991) Evidence for a Paleo-Spreading Center in the Oman Ophiolite: Mantle
1056 Structures in the Maqsad Area. In Springer Netherlands. pp. 147-173.
1057 Ceuleneer G. and le Sueur E. (2008) The Trinity ophiolite (California): The strange
1058 association of fertile. *Bull*. *la Soc*. *Geol*. *Fr*. **179**, 503-518.
1059 Ceuleneer G., Monnereau M. and Amri I. (1996) Thermal structure of a fossil mantle diapir
1060 inferred from the distribution of mafic cumulates. *Nature* **379**, 149-153.
1061 Ceuleneer G., Nicolas A. and Boudier F. (1988) Mantle flow pattern at an oceanic spreading
1062 centre: the Oman peridotite record. *Tectonophysics* **151**, 1-26.
1063 Clénet H., Ceuleneer G., Pinet P., Abily B., Daydou Y., Harris E., Amri I. and Dantas C.
1064 (2010) Thick sections of layered ultramafic cumulates in the Oman ophiolite revealed by
1065 an airborne hyperspectral survey: Petrogenesis and relationship to mantle diapirism.
1066 *Lithos* **114**, 265-281.
1067 Coleman R. G. and Keith T. E. (1971) A chemical study of serpentinization-burro mountain,
1068 California. *J*. *Petrol*. **12**, 311-328.
1069 Collier M. L. and Kelemen P. B. (2010) The case for reactive crystallization at mid-ocean
1070 ridges. *J*. *Petrol*. **51**, 1913-1940.
1071 Daines M. J. and Kohlstedt D. L. (1994) The transition from porous to channelized flow due
1072 to melt/rock reaction during melt migration. *Geophys*. *Res*. *Lett*. **21**, 145-148.
1073 Deschamps F., Godard M., Guillot S. and Hattori K. (2013) Geochemistry of subduction zone
1074 serpentinites: A review. *Lithos* **178**, 96-127.

1075 Dick H. J. B. (1977) Evidence of partial melting in the Josephine peridotite. *Magma Genes*.
1076 **96**, 59-62.
1077 Dick H. J. B., Johan Lissenberg C. and Warren J. M. (2010) Mantle melting, melt transport,
1078 and delivery beneath a slow-spreading ridge: The paleo-MAR from 23°15'N to 23°45'N.
1079 *J*. *Petrol*. **51**, 425-467.
1080 Dick H. J. B. and Natland J. H. (1996) Late-stage melt evolution and transport in the shallow
1081 mantle beneath the East Pacific Rise. *Proc*. *ODP Sci*. *Res*. **147**, 103-134.
1082 Drouin M., Godard M., Ildefonse B., Bruguier O. and Garrido C. J. (2009) Geochemical and
1083 petrographic evidence for magmatic impregnation in the oceanic lithosphere at Atlantis
1084 Massif, Mid-Atlantic Ridge (IODP Hole U1309D, 30°N). *Chem*. *Geol*. **264**, 71-88.
1085 Dygert N., Kelemen P. B. and Liang, Y. (2017) Spatial variations in cooling rate in the mantle
1086 section of the Samail ophiolite in Oman: Implications for formation of lithosphere at
1087 mid-ocean ridges. *Earth Planet*. *Sci*. *Lett*. **465**, 134-144.
1088 Elthon D. (1979) High magnesia liquids as the parental magma for ocean floor basalts. *Nature*
1089 **278**, 514-518.
1090 Faul U. H. (1997) Permeability of partially molten upper mantle rocks from experiments and
1091 percolation theory. *J*. *Geophys*. *Res*. **102**, 10299.
1092 Frey F. A., Green D. H. and Roy S. D. (1978) Integrated models of basalt petrogenesis: A
1093 study of quartz tholeiites to olivine melilitites from South Eastern Australia utilizing
1094 geochemical and experimental petrological data. *J*. *Petrol*. **19**, 463-513.
1095 Gerbert-Gaillard L. (2002) Caractérisation Géochimique des Péridotites de l'ophiolite
1096 d'Oman : Processus Magmatiques aux Limites Lithosphère/Asthénosphère. *PhD Thesis*
1097 Université Montpellier II - Sciences et Techniques du Languedoc, 238 pp.
1098 Ghosh B., Morishita T., Gupta B. Sen, Tamura A., Arai S. and Bandyopadhyay D. (2014)
1099 Moho transition zone in the Cretaceous Andaman ophiolite, India: A passage from the

1100 mantle to the crust. *Lithos* **198–199**, 117-128.
1101 Girardeau J., Monnier C., Le Mée L. and Quatrevaux F. (2002) The Wuqbah peridotite,
1102 central Oman Ophiolite: Petrological characteristics of the mantle in a fossil overlapping
1103 ridge setting. *Mar*. *Geophys*. *Res*. **23**, 43-56.
1104 Godard M., Bodinier J. and Vasseur G. (1995) Effects of mineralogical reactions on trace
1105 element redistributions in mantle rocks during percolation processes : A chromatographic
1106 approach. *Earth Planet*. *Sci*. *Lett*. **133**, 449-461.
1107 Godard M., Bosch D. and Einaudi F. (2006) A MORB source for low-Ti magmatism in the
1108 Semail ophiolite. *Chem*. *Geol*. **234**, 58-78.
1109 Godard M., Dautria J. M. and Perrin M. (2003) Geochemical variability of the Oman
1110 ophiolite lavas: Relationship with spatial distribution and paleomagnetic directions.
1111 *Geochemistry, Geophys*. *Geosystems* **4**.
1112 Godard M., Jousselin D. and Bodinier J. L. (2000) Relationships between geochemistry and
1113 structure beneath a palaeo-spreading centre: A study of the mantle section in the Oman
1114 ophiolite. *Earth Planet*. *Sci*. *Lett*. **180**, 133-148.
1115 Godard M., Lagabrielle Y., Alard O. and Harvey J. (2008) Geochemistry of the highly
1116 depleted peridotites drilled at ODP Sites 1272 and 1274 (Fifteen-Twenty Fracture Zone,
1117 Mid-Atlantic Ridge): Implications for mantle dynamics beneath a slow spreading ridge.
1118 *Earth Planet*. *Sci*. *Lett*. **267**, 410-425.
1119 Green D. H. and Ringwood A. E. (1967) The genesis of basaltic magmas. *Contrib*. *to*
1120 *Mineral*. *Petrol*. **15**, 103-190.
1121 Gruau G., Bernard-Griffiths J. and Lécuyer C. (1998) The origin of U-shaped rare earth
1122 patterns in ophiolite peridotites: assessing the role of secondary alteration and melt/rock
1123 reaction. *Geochim*. *Cosmochim*. *Acta* **62**, 3545-3560.
1124 Hanghøj K., Kelemen P. B., Hassler D. and Godard M. (2010) Composition and genesis of

depleted mantle peridotites from the Wadi Tayin massif, Oman ophiolite; Major and trace element geochemistry, and Os isotope and PGE systematics. *J*. *Petrol*. **51**, 201-227.

Hauri E. H. and Hart S. R. (1995) Correction to "Constraints on melt migration from mantle plumes: A trace element study of peridotite xenoliths from Savai'i, Western Samoa" by Erik H. Hauri and Stanley R. Hart. *J*. *Geophys*. *Res*. *Solid Earth* **100**, 2003-2003.

Herzberg C. T., Fyfe W. S. and Carr M. J. (1983) Density constraints on the formation of the continental Moho and crust. *Contrib*. *to Mineral*. *Petrol*. **84**, 1-5.

Ishikawa T., Fujisawa S., Nagaishi K. and Masuda T. (2005) Trace element characteristics of the fluid liberated from amphibolite-facies slab: Inference from the metamorphic sole beneath the Oman ophiolite and implication for boninite genesis. *Earth Planet*. *Sci*. *Lett*. **240**, 355-377.

Ishikawa T., Nagaishi K. and Umino S. (2002) Boninitic volcanism in the Oman ophiolite: Implications for thermal condition during transition from spreading ridge to arc. *Geology* **30**, 899-902.

Jagoutz E., Palme H., Baddenhausen H., Blum K., Cendales M., Dreibus G., Spettel B., Lorenz V. and Wanke H. (1979) The abundances of major, minor and trace elements in the earth's mantle as derived from primitive ultramafic nodules. *Proc*. *Lunar Planet*. *Sci*. *Conf*. *10th*, 2031-2050.

Jan M. Q. and Howie R. A. (1981) The Mineralogy and Geochemistry of the Metamorphosed Basic and Ultrabasic Rocks of the Jijal Complex, Kohistan, NW Pakistan. *J*. *Petrol*. **22**, 85-126.

Jochum K. P., Weis U., Stoll B., Kuzmin D., Yang Q., Raczek I., Jacob D. E., Stracke A., Birbaum K., Frick D. A., Günther D. and Enzweiler J. (2011) Determination of reference values for NIST SRM 610-617 glasses following ISO guidelines. *Geostand*. *Geoanalytical Res*. **35**, 397-429.

1150 Johan Z., Martin R. F. and Ettler V. (2017) Fluids are bound to be involved in the formation
1151 of ophiolitic chromite deposits. *Eur*. *J*. *Mineral*. **29**, 543-555.
1152 Jousselin D. and Nicolas A. (2000) The Moho transition zone in the Oman ophiolite-relation
1153 with wehrlites in the crust and dunites in the mantle. *Mar*. *Geophys*. *Res*. **21**, 229-241.
1154 Jousselin D., Nicolas A. and Boudier F. (1998) Detailed mapping of a mantle diapir below a
1155 paleo-spreading center in the Oman ophiolite. *J*. *Geophys*. *Res*. *Earth* **103**, 18153-18170.
1156 Kelemen P. B. (1990) Reaction between ultramafic rock and fractionating basaltic magma I.
1157 phase relations, the origin of calc-alkaline magma series, and the formation of discordant
1158 dunite. *J*. *Petrol*. **31**, 51-98.
1159 Kelemen P. B., Dick H. J. B. and Quick J. E. (1992) Formation of harzburgite by pervasive
1160 melt/rock reaction in the upper mantle. *Nature* **358**, 635-641.
1161 Kelemen P. B., Hirth G., Shimizu N., Spiegelman M. and Dick H. J. (1997b) A review of
1162 melt migration processes in the adiabatically upwelling mantle beneath oceanic
1163 spreading ridges. *Philos*. *Trans*. *R*. *Soc*. *A Math*. *Phys*. *Eng*. *Sci*. **355**, 283-318.
1164 Kelemen P. B., Koga K. and Shimizu N. (1997a) Geochemistry of gabbro sills in the crust-
1165 mantle transition zone of the Oman ophiolite: implications for the origin of the oceanic
1166 lower crust. *Earth Planet*. *Sci*. *Lett*. **146**, 475-488.
1167 Kelemen P. B., Shimizu N. and Dunn T. (1993) Relative depletion of niobium in some arc
1168 magmas and the continental crust: partitioning of K, Nb, La and Ce during melt/rock
1169 reaction in the upper mantle. *Earth Planet*. *Sci*. *Lett*. **120**, 111-134.
1170 Kelemen P. B., Shimizu N. and Salters V. J. M. (1995a) Extraction of mid-ocean-ridge basalt
1171 from the upwelling mantle by focused flow of melt in dunite channels. *Nature* **375**, 747-
1172 753.
1173 Kelemen P. B., Whitehead J. A., Aharonov E. and Jordahl K. A. (1995b) Experiments on flow
1174 focusing in soluble porous media, with applications to melt extraction from the mantle. *J*.

1175 *Geophys*. *Res*. *Solid Earth* **100**, 475-496.
1176 Khedr M. Z., Arai S., Python M. and Tamura A. (2014) Chemical variations of abyssal
1177 peridotites in the central Oman ophiolite: Evidence of oceanic mantle heterogeneity.
1178 *Gondwana Res*. **25**, 1242-1262.
1179 Koga K. T., Kelemen P. B. and Shimizu N. (2001) Petrogenesis of the crust-mantle transition
1180 zone and the origin of lower crustal wehrlite in the Oman ophiolite. *Geochemistry*,
1181 *Geophys*. *Geosystems* **2**.
1182 Kogiso T., Tatsumi Y. and Nakano, S. (1997) Trace element transport during dehydration
1183 processes in the subducted oceanic crust: 1. Experiments and implications for the origin
1184 of ocean island basalts. *Earth Planet*. *Sci*. *Lett*. **148**, 193-205.
1185 Lanphere M. A. (1981) K-Ar ages of metamorphic rocks at the base of the Samail Ophiolite,
1186 Oman. *J*. *Geophys*. *Res*. *Solid Earth* **86**, 2777-2782.
1187 Leblanc M. and Ceuleneer G. (1991) Chromite crystallization in a multicellular magma flow:
1188 Evidence from a chromitite dike in the Oman ophiolite. *Lithos* **27**, 231-257.
1189 Lee C. T. A., Harbert A. and Leeman W. P. (2007) Extension of lattice strain theory to
1190 mineral/mineral rare-earth element partitioning: An approach for assessing
1191 disequilibrium and developing internally consistent partition coefficients between
1192 olivine, orthopyroxene, clinopyroxene and basaltic melt. *Geochim*. *Cosmochim*. *Acta* **71**,
1193 481-496.
1194 Lorand J. P. and Ceuleneer G. (1989) Silicate and base-metal sulfide inclusions in chromites
1195 from the Maqsad area (Oman ophiolite, Gulf of Oman): A model for entrapment. *Lithos*
1196 **22**, 173-190.
1197 MacLeod C. J., Johan Lissenberg C. and Bibby L. E. (2013) “Moist MORB” axial
1198 magmatism in the Oman ophiolite: The evidence against a mid-ocean ridge origin.
1199 *Geology* **41**, 459-462.

1200 Malvoisin B. (2015) Mass transfer in the oceanic lithosphere: Serpentinization is not
1201 isochemical. *Earth Planet*. *Sci*. *Lett*. **430**, 75-85.
1202 McKenzie D. and Bickle M. J. (1988) The volume and composition of melt generated by
1203 extension of the lithosphere. *J*. *Petrol*. **29**, 625-679.
1204 McKenzie D. and O'Nions R. K. (1991) Partial melt distribution from inversion of rare earth
1205 element concentrations. *J*. *Petrol*. **32**, 1021-1091.
1206 Le Mée L., Girardeau J. and Monnier C. (2004) Mantle segmentation along the Oman
1207 ophiolite fossil mid-ocean ridge. *Nature* **432**, 167-172.
1208 Monnier C., Girardeau J., Le Mée L. and Polvé M. (2006) Along-ridge petrological
1209 segmentation of the mantle in the Oman ophiolite. *Geochemistry, Geophys*. *Geosystems*
1210 **7**.
1211 Montigny R., Le Mer O., Thuizat R. and Whitechurch H. (1988) K-Ar and Ar study of
1212 metamorphic rocks associated with the Oman ophiolite: Tectonic implications.
1213 *Tectonophysics* **151**, 345-362.
1214 Moores E. M. and Vine F. J. (1971) The Troodos Massif, Cyprus and other Ophiolites as
1215 Oceanic Crust: Evaluation and Implications. *Philos*. *Trans*. *R*. *Soc*. *A Math*. *Phys*. *Eng*.
1216 *Sci*. **268**, 443-467.
1217 Navon O. and Stolper E. (1987) Geochemical consequences of melt percolation: the upper
1218 mantle as a chromatographic column. *J*. *Geol*. **95**, 285-307.
1219 Nicolas A., Bouldier F., Ildefonse B. and Ball E. (2000) Accretion of Oman and United Arab
1220 Emirates ophiolite - Discussion of a new structural map. *Mar*. *Geophys*. *Res*. **21**, 147-
1221 179.
1222 Nicolas A., Ceuleneer G., Boudier F. and Misseri M. (1988) Structural mapping in the Oman
1223 ophiolites: Mantle diapirism along an oceanic ridge. *Tectonophysics* **151**, 27-56.
1224 Nicolle M., Jousselin D., Reisberg L., Bosch D. and Stephant A. (2016) Major and trace

element and Sr and Nd isotopic results from mantle diapirs in the Oman ophiolite: Implications for off-axis magmatic processes. *Earth Planet. Sci. Lett.* **437**, 138-149.

Niu Y. (2004) Bulk-rock major and trace element compositions of abyssal peridotites: Implications for mantle melting, melt extraction and post-melting processes beneath Mid-Ocean ridges. *J. Petrol.* **45**, 2423-2458.

O'Hara M. J. (1965) Primary magmas and the origin of basalts. *Scottish J. Geol.* **1**, 19–40.

Ortoleva P., Chadam J., Merino E. and Sen A. (1987) Geochemical self-organization II: the reactive-infiltration instability. *Am. J. Sci.* **287**, 1008-1040.

Palandri J. L. and Reed M. H. (2004) Geochemical models of metasomatism in ultramafic systems: Serpentinization, rodingitization, and sea floor carbonate chimney precipitation. *Geochim. Cosmochim. Acta* **68**, 1115-1133.

Parkinson I. and Pearce J. (1998) Peridotites from the Izu-Bonin-Mariana Forearc (ODP Leg 125): Evidence for mantle melting and melt-mantle interaction in a supra-subduction zone setting. *J. Petrol.* **39**, 1577-1618.

Paulick H., Bach W., Godard M., De Hoog J. C. M., Suhr G. and Harvey J. (2006) Geochemistry of abyssal peridotites (Mid-Atlantic Ridge, 15°20'N, ODP Leg 209): Implications for fluid/rock interaction in slow spreading environments. *Chem. Geol.* **234**, 179-210.

Pearce J. A., Alabaster T., Shelton A. W. and Searle M. P. (1981) The Oman ophiolite as a Cretaceous arc-basin complex: evidence and implications. *Philos. Trans. R. Soc. London* **300**, 299-317.

Prinzhofer A. and Allègre C. J. (1985) Residual peridotites and the mechanims of partial melting. *Earth Planet. Sci. Lett.* **74**, 251-265.

Prinzhofer A., Nicolas A., Cassard D., Moutte J., Leblanc M., Paris J. P. and Rabinovitch M. (1980) Structures in the new caledonia peridotites-gabbros: Implications for oceanic

1250 mantle and crust. *Tectonophysics* **69**, 85-112.
1251 Python M. and Ceuleneer G. (2003) Nature and distribution of dykes and related melt
1252 migration structures in the mantle section of the Oman ophiolite. *Geochemistry,*
1253 *Geophys*. *Geosystems* **4**.
1254 Python M., Ceuleneer G. and Arai S. (2008) Chromian spinels in mafic-ultramafic mantle
1255 dykes: Evidence for a two-stage melt production during the evolution of the Oman
1256 ophiolite. *Lithos* **106**, 137-154.
1257 Python M., Ceuleneer G., Ishida Y., Barrat J.-A. and Arai S. (2007) Oman diopsidites: a new
1258 lithology diagnostic of very high temperature hydrothermal circulation in mantle
1259 peridotite below oceanic spreading centres. *Earth Planet*. *Sci*. *Lett*. **255**, 289-305.
1260 Python M., Yoshikawa M., Shibata T. and Arai S. (2011) Diopsidites and Rodingites:
1261 Serpentinisation and Ca-Metasomatism in the Oman Ophiolite Mantle. In *Dyke Swarms:*
1262 *Keys for Geodynamic Interpretations* Springer Berlin Heidelberg, Berlin, Heidelberg. pp.
1263 401-435.
1264 Quick J. E. (1981) Petrology and petrogenesis of the Trinity Peridotite, an upper mantle diapir
1265 in the Eastern Klamath Mountains, Northern California. *J*. *Geophys*. *Res*. **86**, 11837-
1266 11863.
1267 Rabinowicz M. and Ceuleneer G. (2005) The effect of sloped isotherms on melt migration in
1268 the shallow mantle: a physical and numerical model based on observations in the Oman
1269 ophiolite. *Earth Planet*. *Sci*. *Lett*. **229**, 231-246.
1270 Rabinowicz M., Ceuleneer G. and Nicolas A. (1987) Melt segregation and flow in mantle
1271 diapirs below spreading centres: evidence from the Oman ophiolite. *J*. *Geophys*. *Res*. **92**,
1272 3475-3486.
1273 Rampone E., Borghini G., Godard M., Ildefonse B., Crispini L. and Fumagalli P. (2016)
1274 Melt/rock reaction at oceanic peridotite/gabbro transition as revealed by trace element

chemistry of olivine. *Geochim*. *Cosmochim*. *Acta* **190**, 309-331.

Rioux M., Bowring S., Kelemen P., Gordon S., Dudás F. and Miller R. (2012) Rapid crustal accretion and magma assimilation in the Oman-U.A.E. ophiolite: High precision U-Pb zircon geochronology of the gabbroic crust. *J*. *Geophys*. *Res*. *Solid Earth* **117**.

Rospabé M. (2018) Etude pétrologique, géochimique et structurale de la zone de transition dunitique dans l'ophiolite d'Oman: Identification des processus pétrogénétiques à l'interface manteau/croûte. *PhD thesis* Université Toulouse III - Paul Sabatier.

Rospabé M., Benoit M. and Candaudap F. (2018) Determination of Trace Element Mass Fractions in Ultramafic Rocks by HR-ICP-MS: A Combined Approach Using a Direct Digestion/Dilution Method and Pre-concentration by Co-precipitation. *Geostand*. *Geoanalytical Res*. **42**, 115-129.

Rospabé M., Ceuleneer G., Benoit M., Abily B. and Pinet P. (2017) Origin of the dunitic mantle-crust transition zone in the Oman ophiolite: The interplay between percolating magmas and high-temperature hydrous fluids. *Geology* **45**, 471-474.

Sanfilippo A., Dick H. J. B. and Ohara Y. (2013) Melt-rock reaction in the mantle: Mantle troctolites from the parecevela ancient back-arc spreading center. *J*. *Petrol*. **54**, 861-885.

Sanfilippo A., Morishita T., Kumagai H., Nakamura K., Okino K., Hara K., Tamura A. and Arai S. (2015) Hybrid troctolites from mid-ocean ridges: Inherited mantle in the lower crust. *Lithos* **232**, 124-130.

Sanfilippo A. and Tribuzio R. (2013a) Building of the deepest crust at a fossil slow-spreading centre (Pineto gabbroic sequence, Alpine Jurassic ophiolites). *Contrib*. *to Mineral*. *Petrol*. **165**, 705-721.

Sanfilippo A. and Tribuzio R. (2013b) Origin of olivine-rich troctolites from the oceanic lithosphere: A comparison between the Alpine Jurassic ophiolites and modern slow spreading ridges. *Ofioliti* **38**, 89-99.

1300 Sanfilippo A., Tribuzio R., Ottolini L. and Hamada M. (2017) Water, lithium and trace
1301 element compositions of olivine from Lanzo South replacive mantle dunites (Western
1302 Alps): New constraints into melt migration processes at cold thermal regimes. *Geochim*.
1303 *Cosmochim*. *Acta* **214**, 51-72.
1304 Sanfilippo A., Tribuzio R. and Tiepolo M. (2014) Mantle–crust interactions in the oceanic
1305 lithosphere: Constraints from minor and trace elements in olivine. *Geochim*. *Cosmochim*.
1306 *Acta* **141**, 423-439.
1307 Savov I. P., Ryan J. G., D'Antonio M., Kelley K. and Mattie P. (2005) Geochemistry of
1308 serpentinized peridotites from the Mariana Forearc Conical Seamount, ODP Leg 125:
1309 Implications for the elemental recycling at subduction zones. *Geochemistry, Geophys*.
1310 *Geosystems* **6**.
1311 Schiano P., Clocchiatti R., Lorand J.-P., Massare D., Deloule E. and Chaussidon M. (1997)
1312 Primitive basaltic melts included in podiform chromites from the Oman Ophiolite. *Earth*
1313 *Planet*. *Sci*. *Lett*. **146**, 489-497.
1314 Snow J. E. and Dick H. J. B. (1995) Pervasive magnesium loss by marine weathering of
1315 peridotite. *Geochim*. *Cosmochim*. *Acta* **59**, 4219-4235.
1316 Sobolev A. (1996) Melt Incusions in Minerals as a source of princple petrological
1317 information. *Petrology* **4**, 209-220.
1318 Stead C. V., Tomlinson E. L., McKenna C. A. and Kamber B. S. (2017) Rare earth element
1319 partitioning and subsolidus exchange behaviour in olivine. *Chem*. *Geol*. **475**, 1-13.
1320 Suhr G., Kelemen P. and Paulick H. (2008) Microstructures in Hole 1274A peridotites, ODP
1321 Leg 209, Mid-Atlantic Ridge: Tracking the fate of melts percolating in peridotite as the
1322 lithosphere is intercepted. *Geochemistry, Geophys*. *Geosystems* **9**.
1323 Sun C. and Liang Y. (2014) An assessment of subsolidus re-equilibration on REE distribution
1324 among mantle minerals olivine, orthopyroxene, clinopyroxene, and garnet in peridotites.

Chem. *Geol*. **372**, 80-91.

Sun S.-S. and McDonough W. F. (1989) Chemical and isotopic systematics of oceanic basalts: implications for mantle composition and processes. *Geol*. *Soc*. *London, Spec*. *Publ*. **42**, 313-345.

Sundberg M., Hirth G. and Kelemen P. B. (2010) Trapped melt in the Josephine peridotite: Implications for permeability and melt extraction in the upper mantle. *J*. *Petrol*. **51**, 185-200.

Takazawa E., Okayasu T. and Satoh K. (2003) Geochemistry and origin of the basal lherzolites from the northern Oman ophiolite (northern Fizh block). *Geochemistry, Geophys*. *Geosystems* **4**.

Tamura A., Morishita T., Ishimaru S. and Arai S. (2014) Geochemistry of spinel-hosted amphibole inclusions in abyssal peridotite: Insight into secondary melt formation in melt-peridotite reaction. *Contrib*. *to Mineral*. *Petrol*. **167**, 1-16.

Tilley C. E., Thompson R. N. and Lovenbury P. A. (2007) Melting relations of some oceanic basalts. *Geol*. *J*. **8**, 59-64.

Tilton G. R., Hopson C. A. and Wright J. E. (1981) Uranium-lead isotopic ages of the Samail Ophiolite, Oman, with applications to Tethyan ocean ridge tectonics. *J*. *Geophys*. *Res*. *Solid Earth* **86**, 2763-2775.

Tippit P. R., Pessagno J. E. A. and Smewing J. D. (1981) The biostratigraphy of sediments in the volcanic unit of the Samail ophiolite. *J*. *Geophys*. *Researc* **86**, 2756-2762.

Toramaru A. and Fujii N. (1986) Connectivity of melt phase in a partially molten peridotite. *J*. *Geophys*. *Res*. *Solid Earth* **91**, 9239-9252.

Van Orman J. A., Grove T. L. and Shimizu N. (2001) Rare earth element diffusion in diopside: influence of temperature, pressure, and ionic radius, and an elastic model for diffusion in silicates. *Contrib*. *to Mineral*. *Petrol*. **141**, 687-703.

1350 Verhoogen J. (1954) Petrological evidence on temperature distribution in the mantle of the
1351 earth. *Eos, Trans. Am. Geophys. Union.*
1352 Vernières J., Godard M. and Bodinier J.-L. (1997) A plate model for the simulation of trace
1353 element fractionation during partial melting and magma transport in the Earth's upper
1354 mantle. *J. Geophys. Res.* **102**, 24771.
1355 Yamasaki T., Maeda J. and Mizuta T. (2006) Geochemical evidence in clinopyroxenes from
1356 gabbroic sequence for two distinct magmatisms in the Oman ophiolite. *Earth Planet. Sci.*
1357 *Lett.* **251**, 52-65.
1358 Yokoyama T., Makishima A. and Nakamura E. (1999) Evaluation of the coprecipitation of
1359 incompatible trace elements with fluoride during silicate rock dissolution by acid
1360 digestion. *Chem. Geol.* **157**, 175-187.
1361 You C. F., Castillo P. R., Gieskes J. M., Chan L. H. and Spivack, A. J. (1996) Trace element
1362 behavior in hydrothermal experiments: Implications for fluid processes at shallow depths
1363 in subduction zones. *Earth Planet. Sci. Lett.* **140**, 41-52.

Figure 1

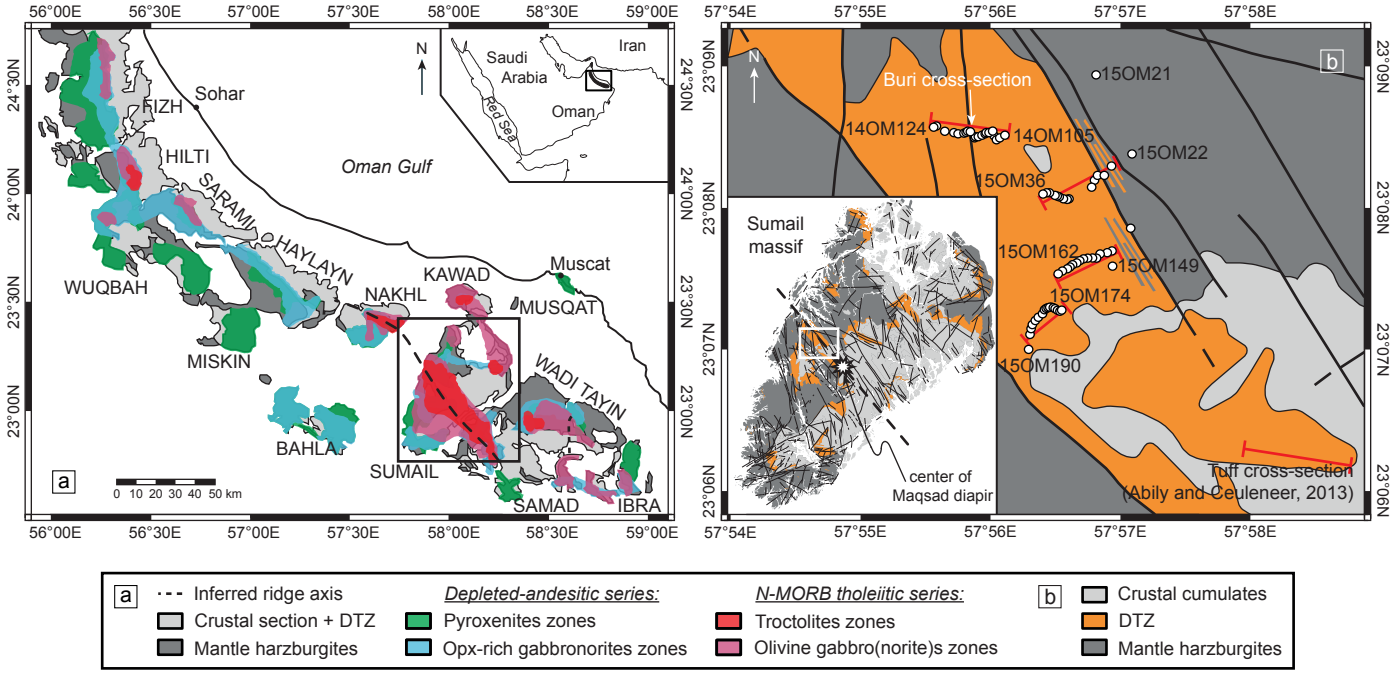

a
- Inferred ridge axis
- Crustal section + DTZ
- Mantle harzburgites

Depleted-andesitic series:
- Pyroxenites zones
- Opx-rich gabbronorites zones

N-MORB tholeiitic series:
- Troctolites zones
- Olivine gabbro(norite)s zones

b
- Crustal cumulates
- DTZ
- Mantle harzburgites

Figure 2

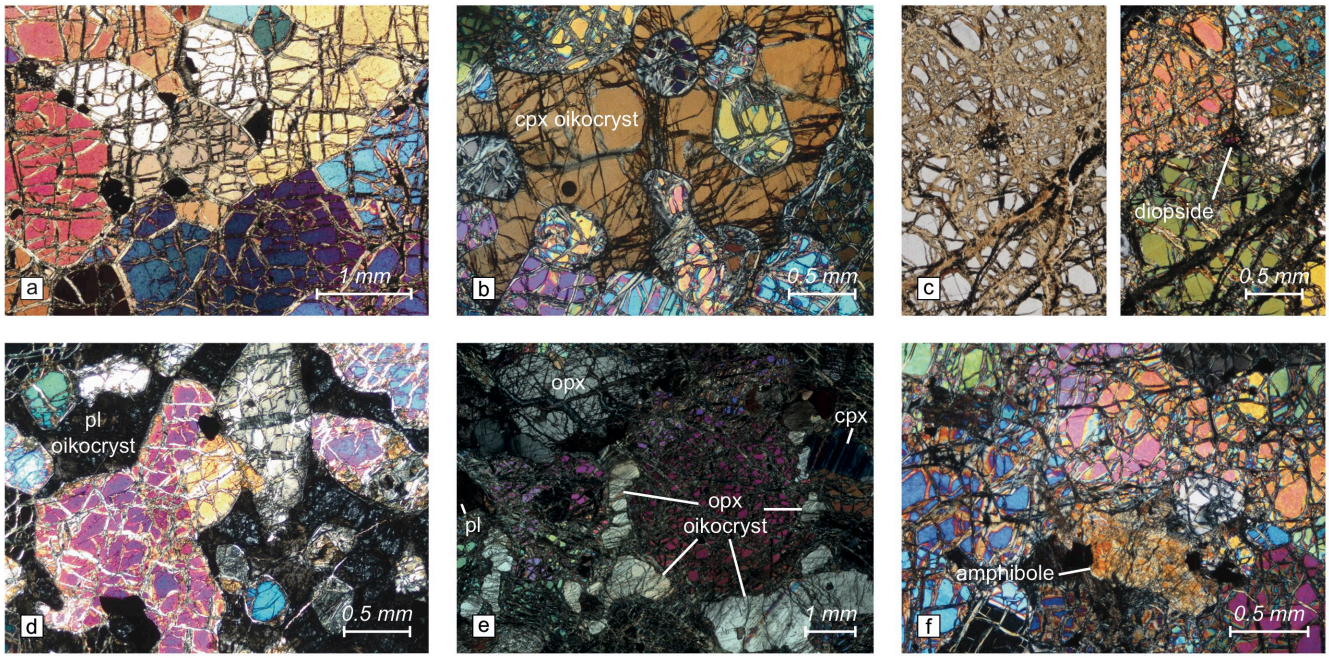
a
1 mm
b
cpx oikocryst
0.5 mm
c
diopside
0.5 mm
d
pl
oikocryst
0.5 mm
e
opx
cpx
pl
opx
oikocryst
1 mm
f
amphibole
0.5 mm

Figure 3

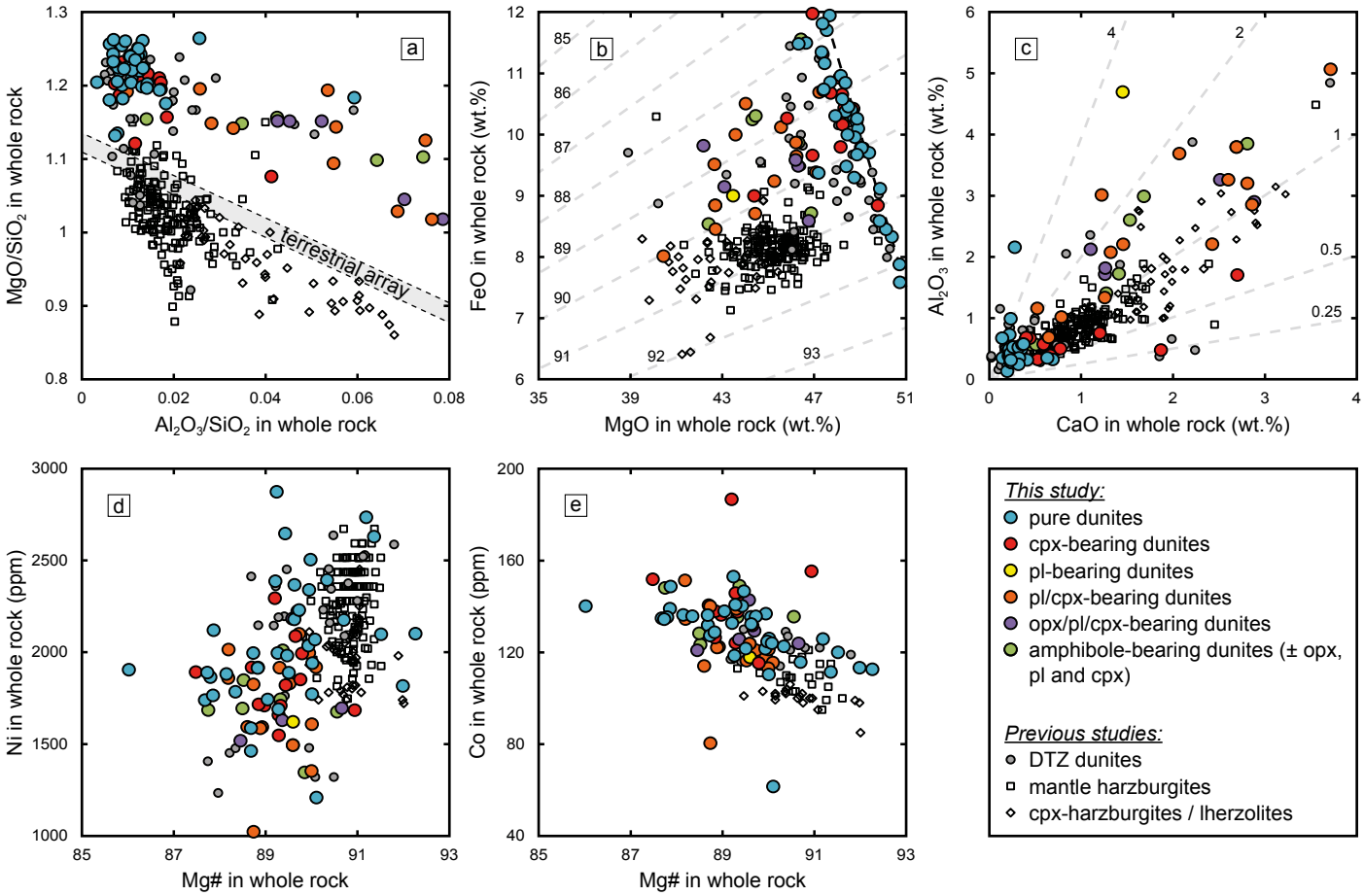
a
b
c
d
e
MgO/SiO2 in whole rock
Al2O3/SiO2 in whole rock
terrestrial array
FeO in whole rock (wt.%)
MgO in whole rock (wt.%)
Al2O3 in whole rock (wt.%)
CaO in whole rock (wt.%)
Ni in whole rock (ppm)
Mg# in whole rock
Co in whole rock (ppm)
Mg# in whole rock
This study:
pure dunites
cpx-bearing dunites
pl-bearing dunites
pl/cpx-bearing dunites
opx/pl/cpx-bearing dunites
amphibole-bearing dunites (± opx, pl and cpx)
Previous studies:
DTZ dunites
mantle harzburgites
cpx-harzburgites / lherzolites

Figure 4

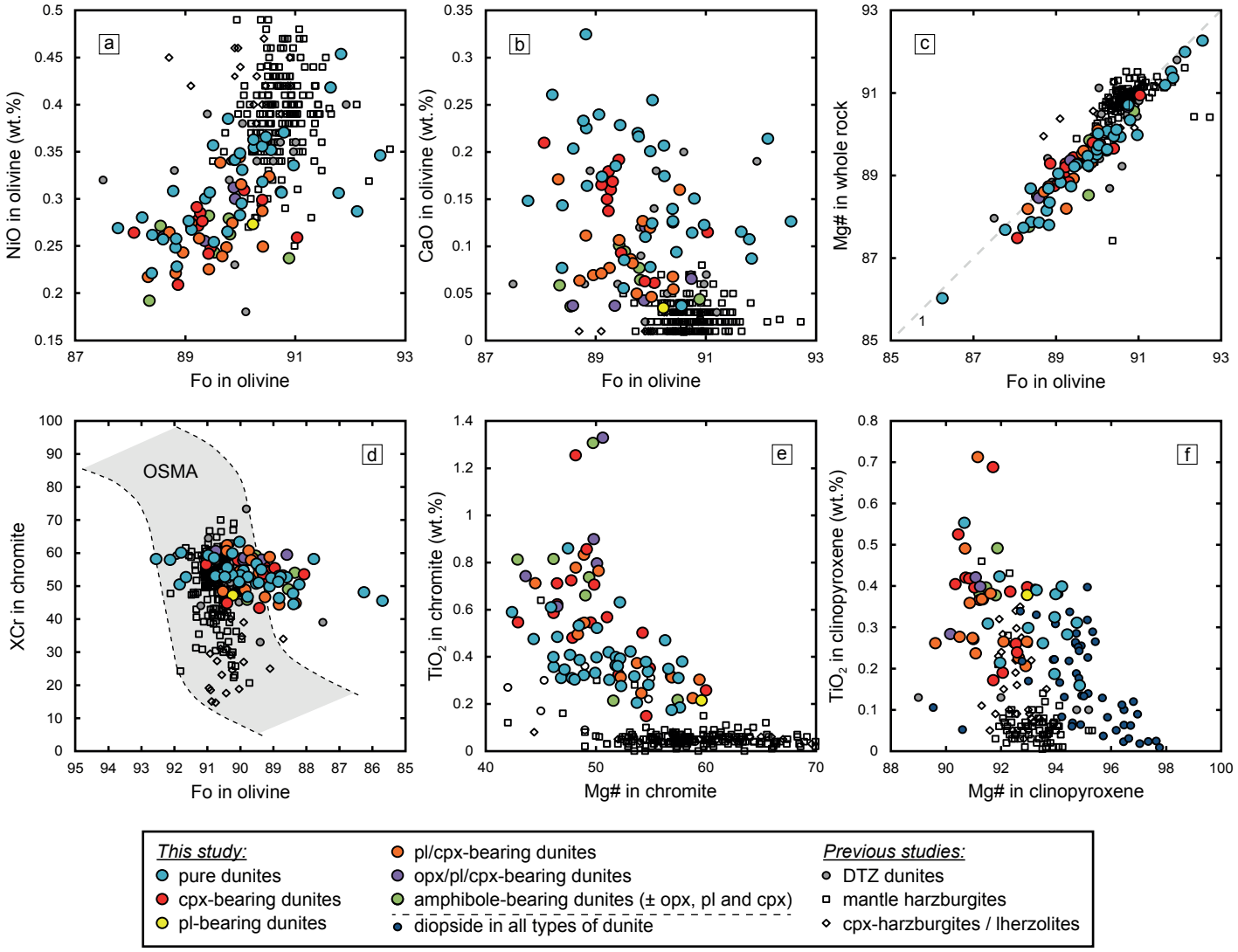
a
NiO in olivine (wt.%)
Fo in olivine
b
CaO in olivine (wt.%)
Fo in olivine
c
Mg# in whole rock
Fo in olivine
1
d
OSMA
XCr in chromite
Fo in olivine
e
TiO2 in chromite (wt.%)
Mg# in chromite
f
TiO2 in clinopyroxene (wt.%)
Mg# in clinopyroxene
This study:
pure dunites
cpx-bearing dunites
pl-bearing dunites
pl/cpx-bearing dunites
opx/pl/cpx-bearing dunites
amphibole-bearing dunites (± opx, pl and cpx)
diopside in all types of dunite
Previous studies:
DTZ dunites
mantle harzburgites
cpx-harzburgites / lherzolites

Figure 5

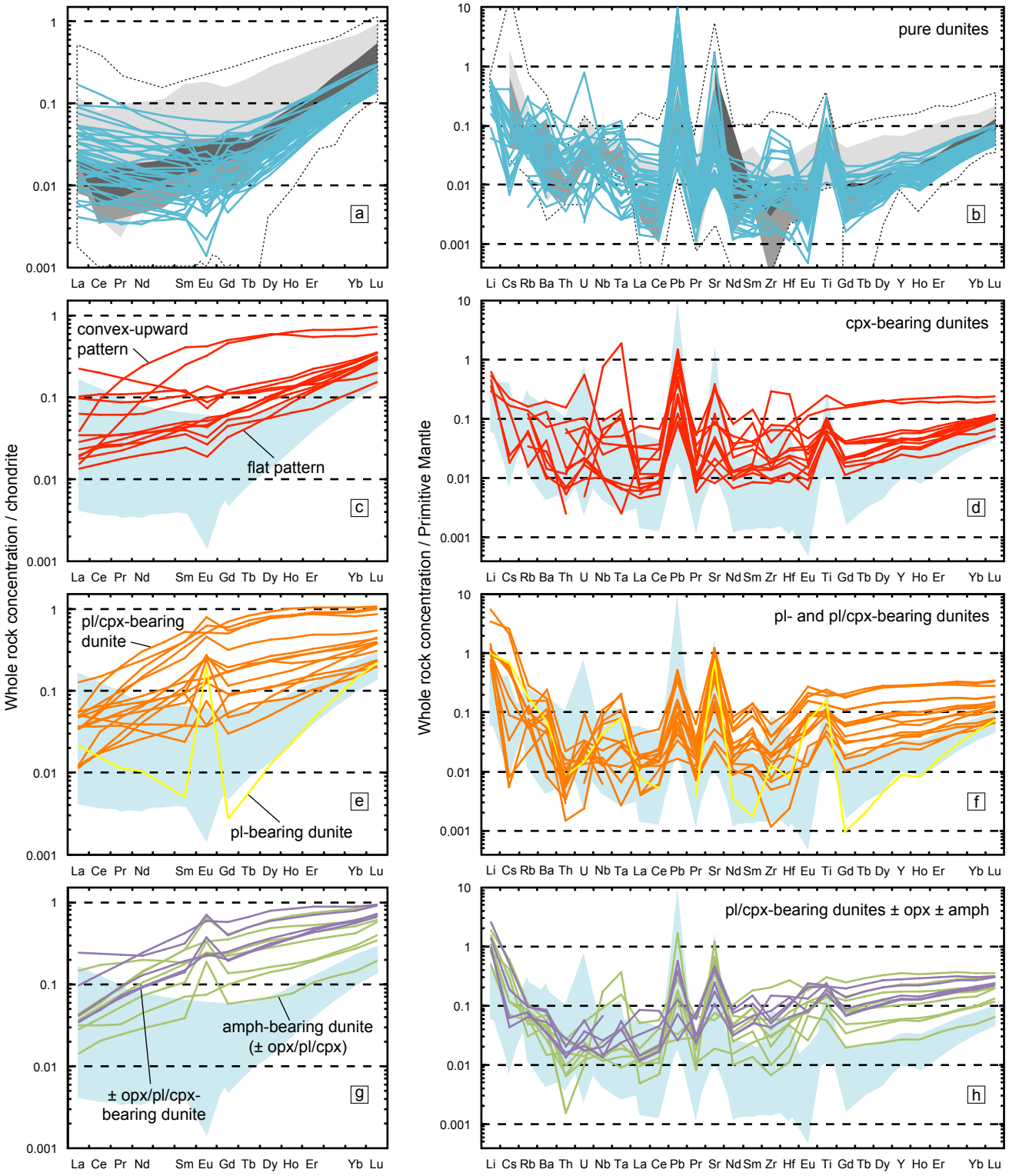
Whole rock concentration / chondrite
Whole rock concentration / Primitive Mantle
a
b
pure dunites
c
convex-upward pattern
flat pattern
d
cpx-bearing dunites
e
pl/cpx-bearing dunite
pl-bearing dunite
f
pl- and pl/cpx-bearing dunites
g
amph-bearing dunite (± opx/pl/cpx)
± opx/pl/cpx-bearing dunite
h
pl/cpx-bearing dunites ± opx ± amph
La Ce Pr Nd Sm Eu Gd Tb Dy Ho Er Yb Lu
Li Cs Rb Ba Th U Nb Ta La Ce Pb Pr Sr Nd Sm Zr Hf Eu Ti Gd Tb Dy Y Ho Er Yb Lu

Figure 6

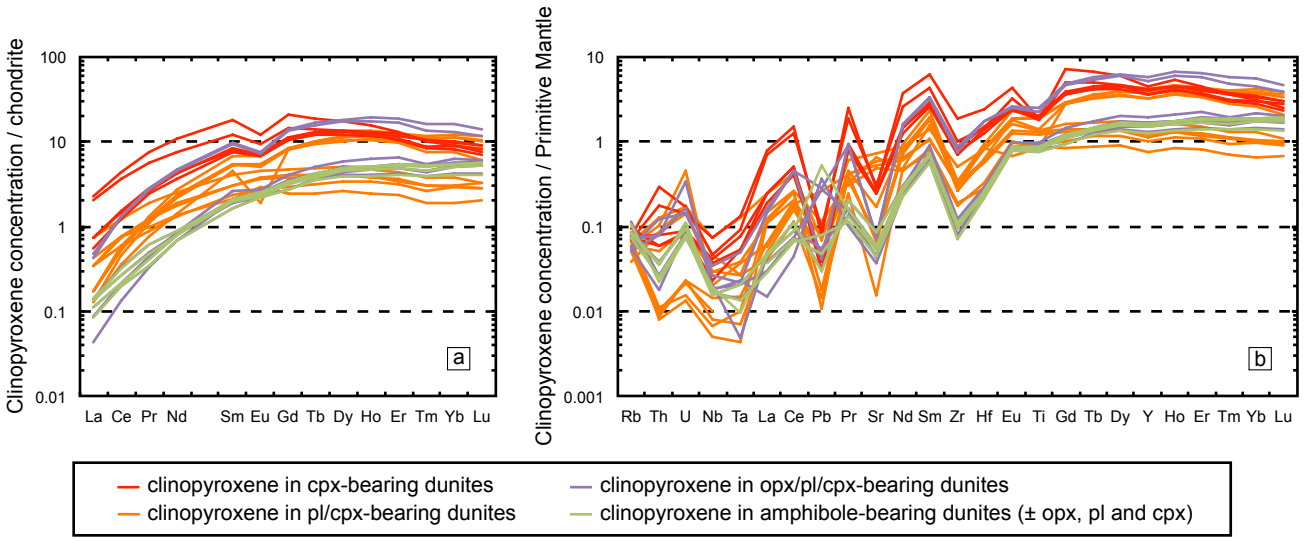
Clinopyroxene concentration / chondrite
100
10
1
0.1
0.01
La Ce Pr Nd Sm Eu Gd Tb Dy Ho Er Tm Yb Lu
a
Clinopyroxene concentration / Primitive Mantle
10
1
0.1
0.01
0.001
Rb Th U Nb Ta La Ce Pb Pr Sr Nd Sm Zr Hf Eu Ti Gd Tb Dy Y Ho Er Tm Yb Lu
b
clinopyroxene in cpx-bearing dunites
clinopyroxene in pl/cpx-bearing dunites
clinopyroxene in opx/pl/cpx-bearing dunites
clinopyroxene in amphibole-bearing dunites (± opx, pl and cpx)

Figure 7

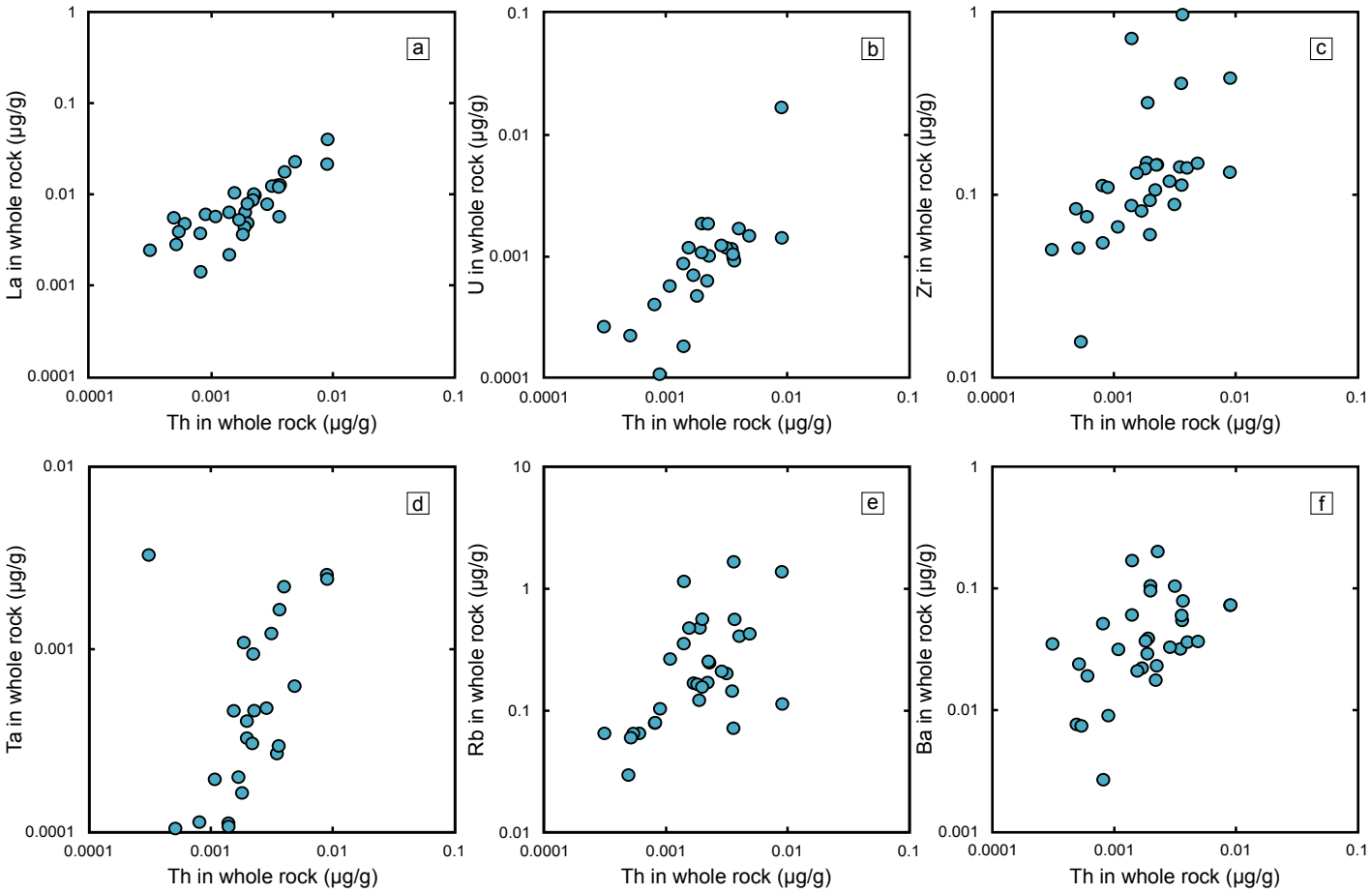
a
La in whole rock (µg/g)
1
0.1
0.01
0.001
0.0001
0.0001
0.001
0.01
0.1
Th in whole rock (µg/g)
b
U in whole rock (µg/g)
0.1
0.01
0.001
0.0001
0.0001
0.001
0.01
0.1
Th in whole rock (µg/g)
c
Zr in whole rock (µg/g)
1
0.1
0.01
0.0001
0.001
0.01
0.1
Th in whole rock (µg/g)
d
Ta in whole rock (µg/g)
0.01
0.001
0.0001
0.0001
0.001
0.01
0.1
Th in whole rock (µg/g)
e
Rb in whole rock (µg/g)
10
1
0.1
0.01
0.0001
0.001
0.01
0.1
Th in whole rock (µg/g)
f
Ba in whole rock (µg/g)
1
0.1
0.01
0.001
0.0001
0.001
0.01
0.1
Th in whole rock (µg/g)

Figure 8

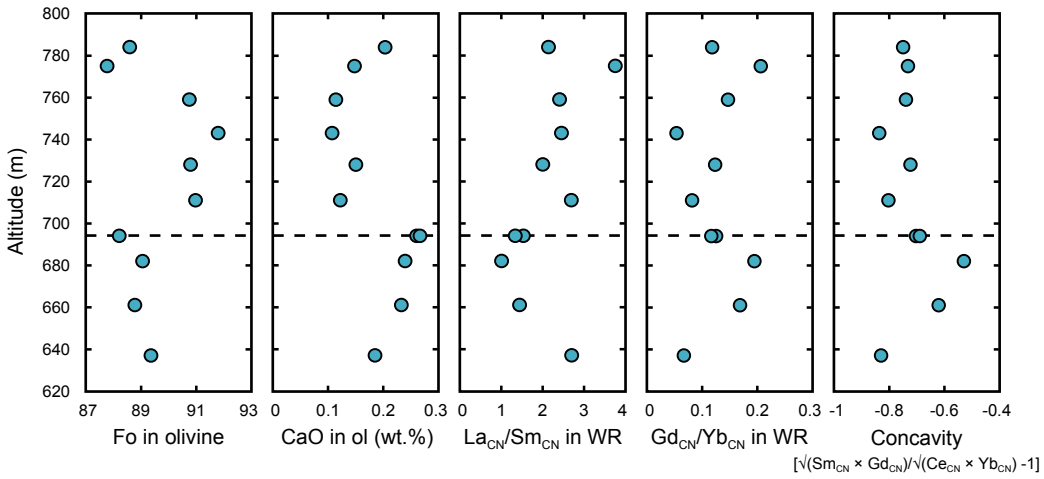
Altitude (m)
800
780
760
740
720
700
680
660
640
620
87
89
91
93
Fo in olivine
0
0.1
0.2
0.3
CaO in ol (wt.%)
0
1
2
3
4
La$_{CN}$/Sm$_{CN}$ in WR
0
0.1
0.2
0.3
Gd$_{CN}$/Yb$_{CN}$ in WR
-1
-0.8
-0.6
-0.4
Concavity
[√(Sm$_{CN}$ × Gd$_{CN}$)/√(Ce$_{CN}$ × Yb$_{CN}$) -1]

Figure 9

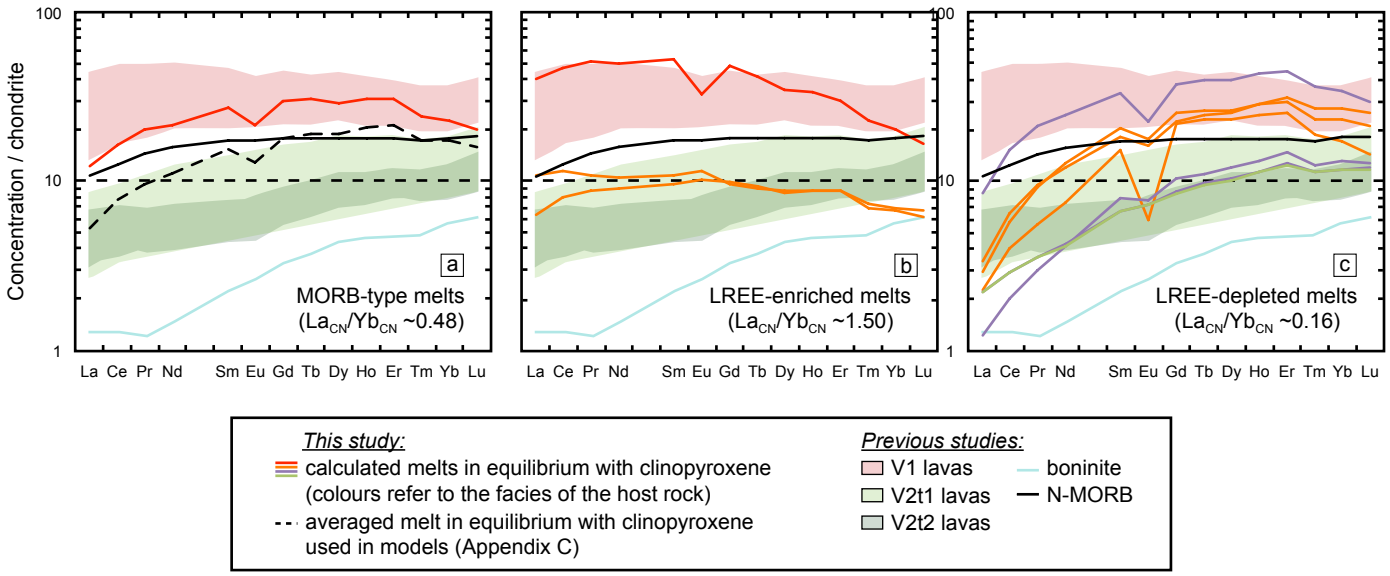
Concentration / chondrite
100
10
1
La Ce Pr Nd Sm Eu Gd Tb Dy Ho Er Tm Yb Lu
a
MORB-type melts
(La$_{CN}$/Yb$_{CN}$ ~0.48)
b
LREE-enriched melts
(La$_{CN}$/Yb$_{CN}$ ~1.50)
c
LREE-depleted melts
(La$_{CN}$/Yb$_{CN}$ ~0.16)
This study:
calculated melts in equilibrium with clinopyroxene
(colours refer to the facies of the host rock)
averaged melt in equilibrium with clinopyroxene
used in models (Appendix C)
Previous studies:
V1 lavas
V2t1 lavas
V2t2 lavas
boninite
N-MORB

Figure 10

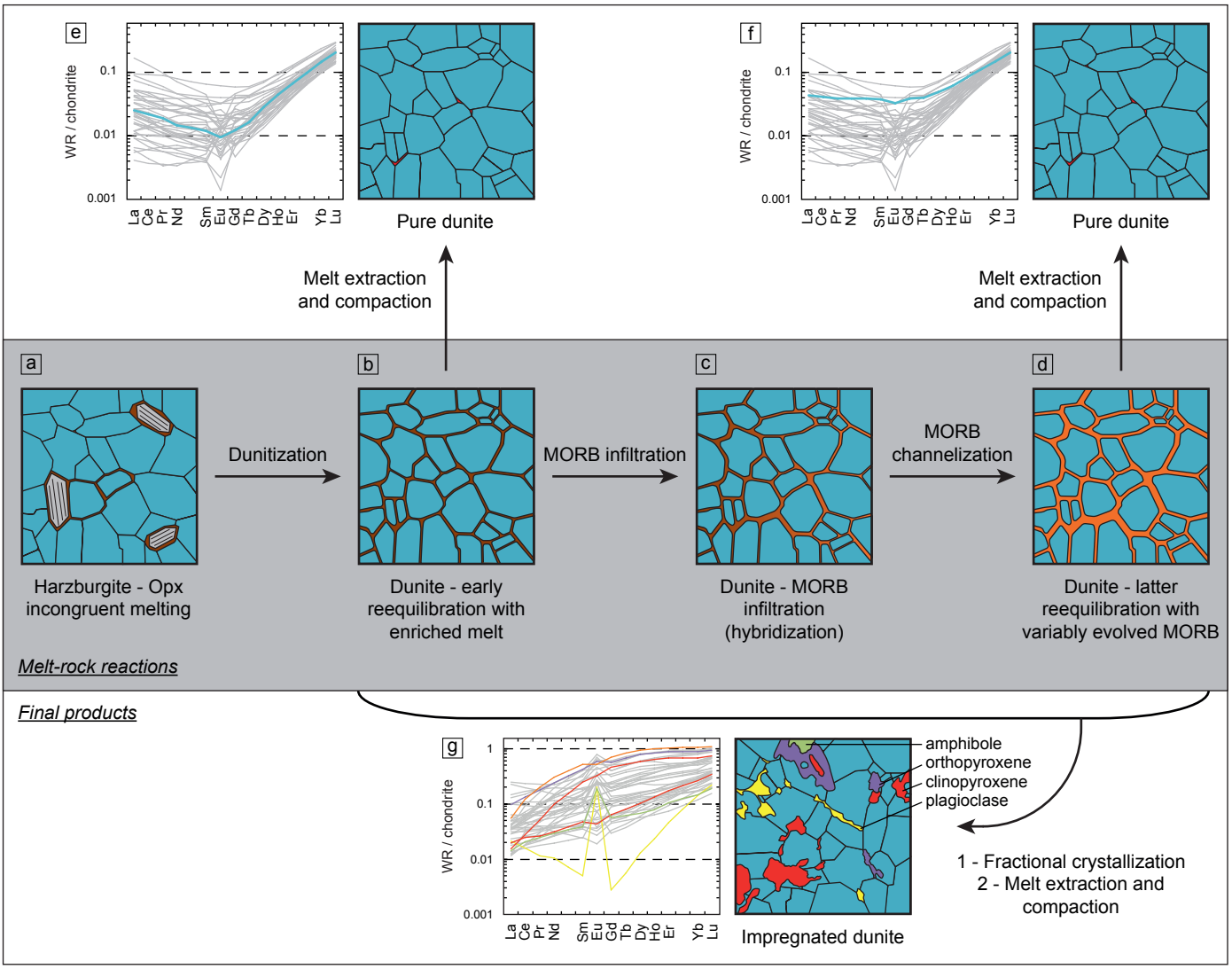
e
WR / chondrite
0.1
0.01
0.001
La Ce Pr Nd Sm Eu Gd Tb Dy Ho Er Yb Lu
Pure dunite
f
WR / chondrite
0.1
0.01
0.001
La Ce Pr Nd Sm Eu Gd Tb Dy Ho Er Yb Lu
Pure dunite
Melt extraction and compaction
Melt extraction and compaction
a
b
c
d
Dunitization
MORB infiltration
MORB channelization
Harzburgite - Opx incongruent melting
Dunite - early reequilibration with enriched melt
Dunite - MORB infiltration (hybridization)
Dunite - latter reequilibration with variably evolved MORB
Melt-rock reactions
Final products
g
WR / chondrite
1
0.1
0.01
0.001
La Ce Pr Nd Sm Eu Gd Tb Dy Ho Er Yb Lu
Impregnated dunite
amphibole
orthopyroxene
clinopyroxene
plagioclase
1 - Fractional crystallization
2 - Melt extraction and compaction